Q. J. R. Meteorol. Soc. (1991), **117**, pp. 207–241 551.574.13:551.577.11

Ice particle concentrations and precipitation development in small polar maritime cumuliform clouds

By ARTHUR L. RANGNO and PETER V. HOBBS

Department of Atmospheric Sciences, University of Washington, Seattle, Washington, U.S.A.

(Received 25 January 1990, revised 30 July 1990)

SUMMARY

Increases in the concentrations of ice particles, as well as precipitation development, can proceed very rapidly in even quite small maritime cumuliform clouds. In the upper portions of these clouds, ice particle concentrations can increase from <1 per litre to >100 per litre in ~10 minutes, even when cloud tops are warmer than −12°C. Just prior to the onset of the high ice particle concentrations in the upper regions of these clouds, a few liquid and frozen drizzle drops appear; these are followed almost immediately by high concentrations of largely vapour-grown ice crystals. Subsequently, the ice particle concentrations gradually decline as the ice particles grow, aggregate and fall out. Crystal habits and sizes indicate that nearly all of the ice crystals encountered in the upper regions of the clouds form close to those regions.

Prior to the formation of high ice particle concentrations, the clouds generally contained, near cloud top, droplets >30 μm diameter in concentrations >1 cm^{-3}, and often drizzle drops (100–400 μm diameter) in concentrations >1 per litre. For maritime and continental cumuliform clouds with widths $D \gtrsim 3$ km, the breadth of the droplet spectrum near the cloud top is a better predictor of the maximum ice particle concentrations that will develop in this region than is cloud-top temperature.

Exceptions to the general picture described above are the very narrow ($D < 3$ km), 'chimney-type', maritime cumuliform clouds with tops that quickly subside after reaching their maximum altitude. For cloud-top temperatures between −7 and −13°C these clouds produce fewer ice particles (~1–20 per litre), even though droplets with diameters >30 μm are present in concentrations >1 cm^{-3} and drizzle drops are often present in concentrations >1 per litre.

Several proposed mechanisms for the formation of high ice particle concentrations in clouds are discussed in the light of these field observations. In a detailed case-study, ice particle concentrations produced by the ejection of ice splinters during riming were calculated to be about an order of magnitude less than the ice particle concentrations measured in the upper regions of the wider maritime clouds. The freezing of evaporating drops by contact nucleation could be responsible for the frozen drops that precede the high concentrations of vapour-grown ice crystals. The latter could be produced in localized regions of unexpectedly high supersaturation that may be produced when drops begin to grow by collisions. This explanation is consistent with several of our findings concerning the conditions under which high concentrations of vapour-grown crystals appear almost spontaneously in maritime clouds. Similarities between these natural crystals, and the conditions under which they appear, and those produced artificially by dry-ice seeding and by aircraft flying through supercooled clouds are discussed.

1. INTRODUCTION

It has long been known that the tops of cumuliform clouds can transform rapidly into ice, producing a cirriform appearance (Clayden 1905). Coons and Gunn (1951) reported on the appearance of ice in the tops of cumulus congestus clouds along the Gulf Coast of the United States, as soon as the cloud-top temperatures fell below about −6°C. Subsequent aircraft studies supported these early reports (e.g. Koenig 1963; Braham 1964; Hallett *et al.* 1978; Hobbs and Rangno 1990). However, the conditions required for such rapid glaciation, and the mechanisms responsible for it, are still not clear (e.g. Mossop 1985a).

The source of the enigma can be traced to measurements, starting in the 1940s, which indicated that ice-forming nuclei in the atmosphere are quite rare. An empirical relationship that fits several such sets of measurements is (Fletcher 1962)

$$n(\Delta T) = n_0 \exp(\beta \Delta T) \tag{1}$$

where $n(\Delta T)$ is the concentration of ice nuclei (per litre) active at supercooling $\leq \Delta T$,

$n_0 = 10^{-5}$ per litre and $\beta = 0.6$. Based on this expression, the concentration of ice particles that form in a cloud by heterogeneous nucleation should be about 1 per litre at −20°C and negligible at temperatures above about −10°C. Direct measurements in clouds, on the other hand, have shown concentrations of 1–100 per litre at cloud-top temperatures >−10°C (e.g., Koenig 1963; Braham 1964; Mossop *et al.* 1968; Hobbs 1969, 1974; Hobbs and Atkinson 1976; Mossop 1985b; Hobbs and Rangno 1985). In particular, maritime cumulus clouds and continental clouds containing drizzle or larger supercooled drops show a propensity for high ice particle concentrations (e.g. Koenig 1963; Braham 1964; Hallett *et al.* 1978; Mossop 1985a; Hobbs and Rangno 1985). The phenomenon of ice particle concentrations that are significantly in excess of those expected from Eq. (1) is referred to as ice multiplication or ice enhancement (Hobbs 1969).

The work described in this paper is a continuation of a study of ice in clouds, the initial results of which were reported by Hobbs and Rangno (1985, 1987)—hereafter referred to as HR. HR concluded that high ice particle concentrations formed in a variety of maritime and continental cumulus clouds with tops between about −6 and −32°C provided that the cloud droplet spectrum was sufficiently broad in the younger cloud portions preceding the formation of ice. Ice enhancement was observed to occur not only in clouds that largely met the riming–splintering criteria (Hallett and Mossop 1974; Mossop 1985c), but also in clouds that did not.

In this paper we present a new data-set on ice particle concentrations in small maritime cumuliform clouds. Owing to the addition of several types of measurements aboard the research aircraft (ice nuclei, ice crystals collected by impaction, video camera records, and 35 GHz radar data), higher data resolution and the extension of our observations to additional sizes of maritime cumuli, some new insights have been obtained into the phenomenon of ice enhancement and its role in the formation of precipitation in maritime cumulus clouds. This new data-set will be described, compared to that of HR, and used to evaluate several theories that have been proposed to explain ice enhancement.

2. Observational facilities and methods of analysis

The measurements and observations described in this paper were obtained aboard the University of Washington's (UW) Convair C-131A research aircraft.

Ice nucleus concentrations were measured using the millipore filter technique (Rosinski and Morgan 1988). The filters had a 0.22 μm pore size. Outside air was drawn isokinetically into the aircraft and through the filters at a rate of about 17 litres per minute. A minimum of 100 litres of air was drawn through each filter, although sometimes as much as 500 litres of air was sampled. To maximize the amount of filter surface available for analysis, the filters were exposed to the air in pairs. One pair of filters was generally exposed from about 30 m above the ocean surface up to cloud base, and two pairs of filters were exposed near the cloud top. For each flight a pair of 'control' filters were handled in the same manner as the other filters, except that air was not drawn through them. The filters were analysed in the laboratory (by Dr J. Rosinski) for ice nucleus concentrations by exposing them to low water-vapour supersaturations (<1%) and various temperatures, then counting the number of crystals that appeared on the filters. In some cases, the crystals that appeared were evaporated by passing air over the filter, and then the filter was again exposed to supersaturated air at various temperatures to see how many new crystals appeared on the filter. This cycle was repeated several times.

Ice particle concentrations in the clouds were measured with Particle Measuring Systems (PMS) 2-D cloud and precipitation probes (Knollenberg 1981). The 2-D cloud probe has a detection limit of ~0.02 per litre for particles >50 μm diameter. However, since it is difficult to determine the nature of particles $\lesssim$100 μm, in maximum dimension, from the 2-D imagery, ice particle concentrations derived from this probe were tabulated only for particles with maximum dimensions $\geq$100 μm (compared to $\geq$150 μm used by HR). Also, in the present study we counted those particles that contacted only one side of the diode array of the 2-D PMS instruments, as well as those that were wholly within the diode array or spanned it completely. The assumption used in counting particles that touched one side of the diode array was that about 50% of all such particles have their centres within the sampling volume. This assumption was supported by scrutiny of a considerable amount of PMS 2-D imagery. 'Streakers', as well as some other PMS 2-D artefacts, were eliminated by requiring that the perimeter/area ratio be $\geq$0.85 when quasi-spherical ice particles (e.g., plates, stellars, graupel, drizzle-drops) were present and $\geq$1.5 for thin columnar particles.

When applied to the clouds studied by HR, the changes in procedures for analysing the PMS imagery described above resulted in an average increase in ice particle concentrations by about a factor of two; about half of this increase was due to counting smaller particles, and the other half to counting particles with images that touched one side of the diode array. However, because, (i) we do not count ice particles $\leq$100 μm in maximum dimension, (ii) we have not corrected for the decreased sample volume in the PMS 2-D cloud probe for particles <162 μm, and (iii) ice crystal aggregates were counted as one particle, the concentrations of ice particles quoted in this present study are still quite conservative (i.e. low compared to the actual concentrations that must have been present in the clouds).

The ice particles seen in the PMS 2-D imagery were broadly classified into columnar, quasi-spherical, and stellars or dendrites. Columnar refers to rod-like ice crystals (columns, needles and sheaths), quasi-spherical to frozen drops, graupel, graupel-like snow and small plates, and stellars or dendrites to ice particles with long feathery extensions and their aggregates.

Ice particle concentrations were also measured with the University of Washington's optical ice-particle counter—OIPC (Turner *et al.* 1976). HR found that the ice particle concentrations measured with the OIPC were highly correlated ($r = 0.9$) and nearly equal in concentrations to those of ice particles $\geq$150 μm in size derived from the 2-D cloud probe. However, in the present work, owing to counting more and smaller crystals in the 2-D imagery, ice particle concentrations measured with the OIPC near the cloud tops, where the ice particles were small, were often less than those derived from the 2-D cloud probe (cf. Turner *et al.* 1976). Nevertheless, the correlation coefficient between the two sets of measurements remained high ($r = 0.8$).

Owing to the sampling of many small clouds and cloud-top tufts only a few hundred metres wide in this study, ice-particle-concentration maxima are given for 2–5 s segments, which correspond to horizontal distances of ~150–300 m (rather than the 1 km segments used by HR).

Cloud particle replicas were obtained by exposing glass slides coated with Formvar to the airstream from one and, occasionally, two locations aboard the aircraft. One location was just behind the pilot's seat where slides, mounted on a rod, could be passed through a hole in the fuselage into a small decelerator through which the outside air passed. This decelerator, which was the same as that described by Hobbs and Farber (1972), decelerated the air to about 20% of the true airspeed. This reduced the fragmentation of ice particles on the slide. The other sampling location (the one most often

used) was located inside the aircraft. It consisted of a man-sized wooden box through which outside air flowed continuously. Outside air flowed into the box through a 2 m long, 9 cm diameter tube with a 5 cm inlet and a 10 cm outlet into the box. Airflow in the box was generally about 15–20 m s^{-1}.

The replicas of ice crystals obtained on the glass slides were examined under a microscope in the laboratory. This helped to improve crystal-habit assignment, the determination of the sizes of the smallest ice crystals collected, and to establish whether small particles were liquid or ice. For example, hexagonal plates $<100\,\mu$m diameter are virtually indistinguishable from droplets in the PMS 2-D imagery, but replicas of ice particles down to about $10\,\mu$m diameter could be distinguished on a slide when viewed under a microscope. Most of the crystals replicated were $\leq 300\,\mu$m in maximum dimension. The smallest crystals replicated were about $10\,\mu$m but such small crystals were rare. The number of crystals on a slide correlated roughly with the concentration of crystals derived from the PMS 2-D cloud probe.

A PMS forward-scattering spectrometer probe (FSSP) (Knollenberg 1981) was used to size cloud particles from 2–47 μm diameter. Glass-bead calibrations have suggested, however, that the upper size limit is closer to 48–51 μm (cf. Heymsfield and Hjelmfelt 1984). Therefore, adjustments proportional to this correction were applied to the FSSP data. Following HR, the broadness of the cloud droplet spectrum will be represented by a 'threshold diameter' (D_T), defined so that the total concentration of droplets with diameters $\geq D_T$ is 3 cm^{-3} as measured by the FSSP. To reduce the effects of ice crystals in artificially broadening the tail of the FSSP spectrum, HR determined D_T from droplet spectra measured in regions of cloud where the OIPC ice particle concentrations were <10 per litre. In this paper, an OIPC ice-particle threshold of <1 per litre is used, although this change in criteria did not greatly affect the value of D_T. As in HR, D_T was calculated from the droplet spectra measured in cloud regions where the liquid water content was at least, and generally much greater than, 0.3 g m^{-3}. Thus, the D_T values were generally derived from droplet spectra measured in the youngest portions of the clouds prior to the development of high ice particle concentrations.

A camera, connected to a video recorder, was positioned just behind the windscreen of the aircraft. In addition to providing a view of the clouds to be sampled, this camera indicated the types of larger cloud and precipitation particles striking the windscreen and, in many cases, whether the turret being approached was rising or falling. Because of the relatively large area ($\sim 25\,cm^{-2}$) of the windscreen viewed by this camera, it provided a sensitive method for detecting larger particles present in low concentrations.

A 35 GHz ($\lambda = 0.86$ cm) radar was aboard the aircraft. This radar could be switched either to an upward-pointing or to a downward-pointing antenna. The radar provides important information on ice fallstreaks and precipitation zones within clouds (Hobbs *et al.* 1985). *In situ* studies of the clouds detected by radar indicated that it can detect particles with maximum dimensions $\gtrsim 100\,\mu$m when they are present in concentrations $\gtrsim 1$ per litre. The 'silent' zone of the radar extended approximately 250 m above or below the aircraft.

The lowest temperature observed in a pass at cloud top was taken to be the cloud-top temperature. This value was subsequently rounded to the next lower 0.5 degC increment (e.g. $-7.2\,°C$ became $-7.5\,°C$). If the cloud-top temperature was not measured directly, the lowest temperature measured during the pass closest to the cloud top was extrapolated (moist-adiabatically) to the cloud-top height to derive a cloud-top temperature. When cloud tops were more than about 300 m above the aircraft, a range of estimated cloud-top temperatures will be quoted. In the figures, the centre value is used to denote cloud-top temperature (e.g. $-13.5 \pm 2\,°C$ is plotted as $-13.5\,°C$). The

temperature at the very highest knob of a turret was often taken to be the cloud-top temperature, even if most of the turret top was 0.5–1 degC warmer. In general, therefore, the cloud-top temperatures reported here are biased, if anything, towards the low-temperature side.

Liquid water content was measured with a Johnson-Williams hot-wire instrument.

3. Location of measurements, cloud types studied and methods of sampling

All of the measurements discussed in this paper were obtained in the western regions of the Puget Sound and over the north-eastern Pacific Ocean up to about 150 km from the Washington coast. The period of the field study was from 30 January 1987 through to 14 March 1990.

The clouds were small (nearly all about 1–3 km deep) cumulus or cumulonimbus that formed in cold and (with one exception) on-shore flow in polar airstreams. The equivalent potential temperatures (θ_e) were, with one exception, in the range 290–310 K. The advantage of sampling such small clouds is that overall updraughts are generally modest ($<5\,m\,s^{-1}$) and in most cases dwindle to zero or become downdraughts when the cloud is just 2–3 km thick. Cloud-base temperatures were, with exceptions on three days, between 0 and 6 °C. The tops of the clouds, which were generally below 4 km above sea level (a.s.l.), had temperatures between −3 and −24 °C, although >95% were warmer than −15 °C. These clouds are particularly suitable for studying ice enhancement since, despite their modest sizes, high ice particle concentrations often form in them and much of the cloud can be sampled quickly.

Droplet concentrations were low (averaging $80\,cm^{-3}$) and fairly uniform (standard deviation $20\,cm^{-3}$) from flight to flight. Drizzle-size drops (100–400 μm diameter) were usually present in the upper, and particularly in the decaying, portions of these clouds, but they never attained millimetric size in the middle and upper cloud portions where the clouds were supercooled.

We sampled cumulus and cumulonimbus clouds with widths (D) in their upper regions $\gtrsim$3 km. These clouds often contained several to many turrets, which were in various stages of development. We also sampled much more slender cumulus clouds (D down to 0.2 km) with shorter-lived and usually descending cloud tops. We will refer to clouds with $D < 3$ km as 'chimney-type'. Figure 1 illustrates the visual differences between these two types of clouds.

Flights were carried out when satellite imagery showed scattered or broken cumuliform clouds over the Pacific coastal waters of Washington State. The most isolated clouds, with top temperatures between −6 and −15 °C, were selected for sampling, although some warmer and colder clouds were encountered. The wider cloud complexes were generally sampled while *en route* to the research area offshore.

In common with other aircraft (Rangno and Hobbs 1983, 1984), we have observed that the Convair C-131A can itself produce localized concentrations of ice particles of hundreds per litre at temperatures $\lesssim$−10 °C, and apparently a few per litre of ice particles at temperatures between −4 to −7 °C. Several tactics were employed to avoid 'contaminating' our measurements with these aircraft-produced ice particles (APIPs). One technique was to sample several cloud tops in their dissipating stage while moving progressively upwind into younger portions of the cloud. Another method used to avoid APIPs was to make two or three passes as quickly as possible at or near the cloud top, with one pass at right angles to the other two. In this way, if APIPs were intercepted, they were in extremely localized regions of the cloud and could be readily identified in the PMS 2-D imagery. Large changes in flight level, from one pass to the next, were also

Figure 1. Photograph showing two types of ice-forming, maritime, cumuliform clouds. (A) Wider clouds even when isolated, produce hundreds per litre of ice particles. (B) Slimmer, short-lived ('chimney-type') clouds with subsiding tops produce fewer ice particles.

used to avoid APIPs. Finally, in postflight analysis, uniformly-sized ice particles in high concentrations in the PMS 2-D imagery in regions close to previous flight tracks, and whose size implicated the aircraft, were excluded from analysis.

In some cases prior to the *in situ* sampling of a cloud, the aircraft was flown above the cloud to monitor it with the downward-pointing radar. Cloud sampling generally began with the aircraft making two or three passes near cloud top. At least one pass near cloud top was directed along the shear line of the cloud (if visibly present) in order to intercept both newly rising and aging portions of the cloud in the same pass. In many cases, however, the cloud top was a quasi-symmetrical, newly risen, first single turret without a clearly defined down-shear aging portion.

Following the passes at cloud top, the aircraft descended in steps of ~300–600 m to cloud base. Eventually, a pass was made ~30 m above the ocean surface to measure ice nucleus concentrations and to establish a temperature–dewpoint sounding profile in the sub-cloud layer. This pass was generally several kilometres away from any precipitating cloud.

Another isolated cloud would then be selected for study, and the above sampling procedure carried out in reverse as the aircraft climbed from cloud base to cloud top. At a propitious point in the flight, a climb to ~0.3 to 1 km above cloud top was often made to establish the characteristics of the environmental air that might be entrained into the cloud top and to make additional ice-nucleus measurements.

4. Results[1]

(*a*) *Ice-nucleus measurements*

An account of the ice-nucleus measurements will be given elsewhere (J. Rosinski—personal communication). Here we are interested only in the maximum measured values (which were generally achieved on the first or second condensation in a series of condensation/evaporation cycles in the developing chamber). The maximum measured ice nucleus concentrations varied from a low of 0.1 per litre at −19 °C to a maximum of 3.2 per litre at −13 °C. The former value is about an order of magnitude less than that given by Eq. (1) and the latter value is about 300 times greater. However, as we shall see in subsection (*c*) below, even the highest measured ice nucleus concentration is less by a factor of ~100 than the maximum ice particle concentrations that we commonly measured in the upper regions of maritime cumuliform clouds that have top temperatures as high as −6 °C.

(*b*) *Concentrations of ice particles during the life-cycle of the clouds*

Figure 2 shows the maximum concentration of ice particles in young, rising (Fig. 2(a) and 2(c)) and in old, dissipating (Fig. 2(b) and 2(d)) maritime cumulus and cumulonimbus clouds. Young, rising clouds were those that had a firm, 'cauliflower' appearance without 'frayed' edges, and which were either still rising or had just reached their maximum heights. Dissipating clouds were those that had ragged and frayed edges, were losing their cumuliform detail, dissolving and in descent, or were even stratiform in appearance (e.g. altostratus cumulonimbogenitus, see cloud A in Fig. 1): they usually contained a great deal of ice. It can be seen from Fig. 2 that relatively little ice was found in the young rising turrets, while high ice particle concentrations were usually present in the dissipating clouds. The very highest ice particle concentrations were generally found >50 m below the top of the aging portions of a cloud (Fig. 2(d)). The time for the visual microstructural transition to occur is less than 10 min, beginning from the time the rising turret nears its maximum height.

It can be seen from Fig. 2(d) that for cloud-top temperatures from about −5 to −24 °C the maximum ice particle concentrations that eventually develop in small polar maritime cumuliform clouds are poorly correlated ($r = 0.31$) with cloud-top temperature. Instead, ice particles appear rather suddenly when the cloud-top temperature falls to −8 ± 2 °C, and thereafter the ice particle concentrations increase quickly to tens or hundreds per litre irrespective of cloud-top temperature (compare, for example, ice particle concentrations for older clouds with tops between −5 and −15 °C—Fig. 2(b) and 2(d)).

(*c*) *Maximum ice particle concentrations and the breadth of the droplet spectrum*

Shown in Fig. 3 are the maximum concentrations of ice particles (I_M) versus the droplet threshold diameter (D_T) for the measurements obtained in the present study and also, for comparison, from the measurements by HR for maritime, continental and

[1] A complete tabulation of our new data-set for maritime clouds (which comprises more than 400 clouds and turrets) may be obtained from the authors.

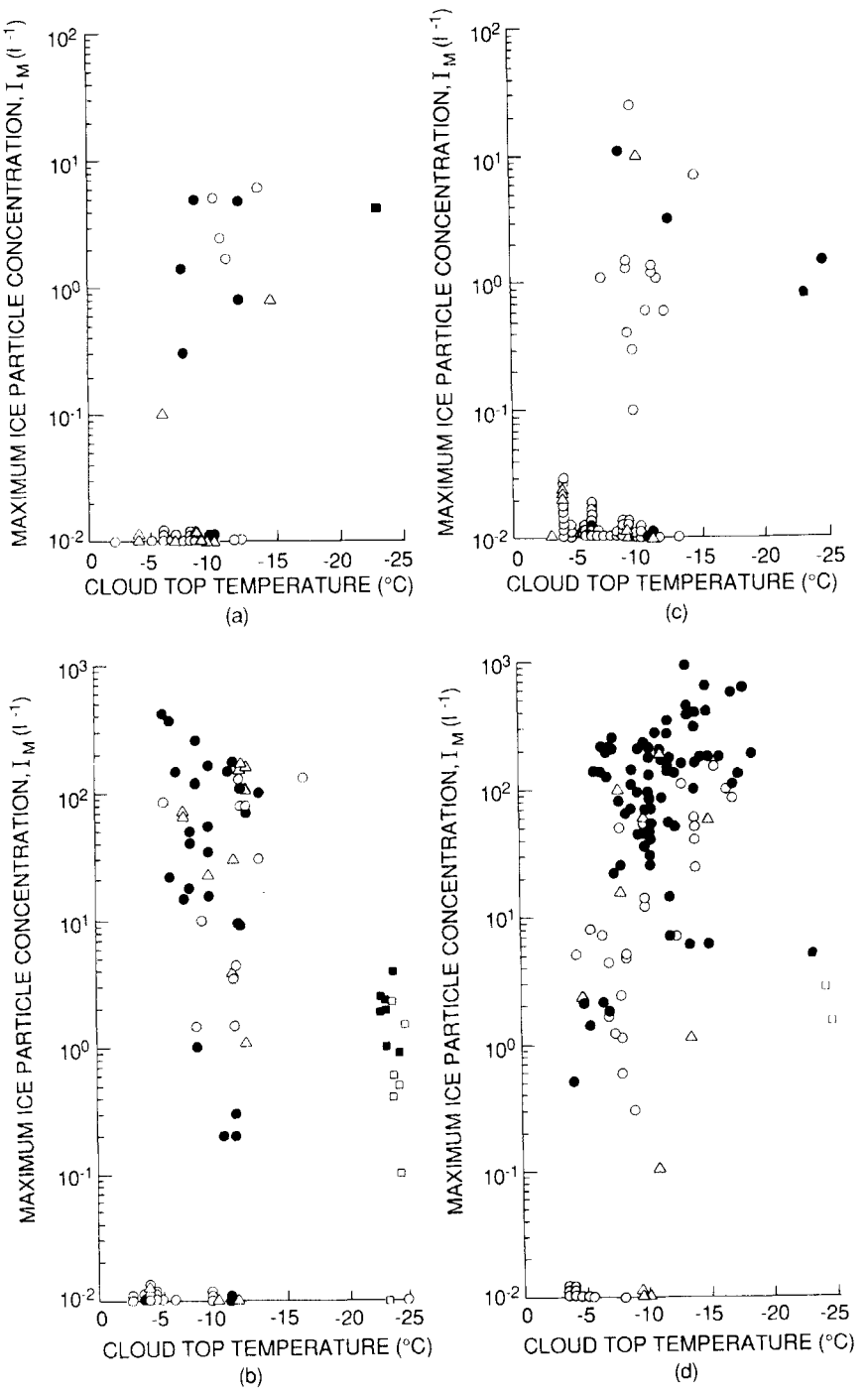

Figure 2. Maximum ice particle concentrations measured in maritime cumuliform clouds: (a) within 50m of the tops of young, rising cloud; (b) within 50m of the tops of old, dissipating clouds; (c) greater than 50m from the tops of young, rising clouds; and (d) greater than 50m from the tops of old, dissipating clouds. Solid circles denote clouds with $D > 3$km. Open circles denote clouds with $D \leq 3$km. Triangles denote clouds where radar data was not available. The square data points in (d) are for 3 February 1989 (see section 4).

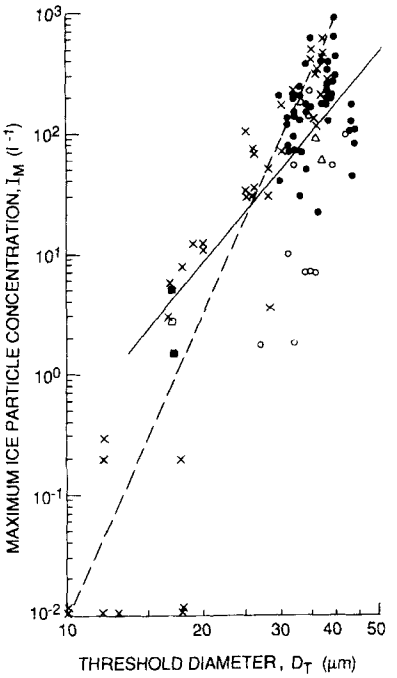

Figure 3. Maximum ice particle concentrations I_M versus droplet threshold diameter D_T (both on logarithmic scales) for mature and aging maritime cumuliform clouds with cloud top temperatures $\leq -6°C$. The circles are new data for the maritime cumuliform clouds discussed in this paper. Solid circles are for clouds with $D > 3$km, and open circles for clouds with $D \leq 3$km. The square data points are for 3 February 1989 (see section 4). Crosses are from Hobbs and Rangno (1985) for maritime, continental and transitional cumuliform clouds. The dashed line is the concentration of ice particles given by Eq. 2 from Hobbs and Rangno (1985) and the solid line is for the new data presented in this paper (see section 4).

transitional cumuliform clouds (which have been reprocessed using the criteria described in section 3 for those clouds for which PMS 2-D cloud probe imagery was available).

For dissipating clouds with tops $\leq -6\,°C$ that were sampled at more than 50 m below cloud top, the empirical relationship ($r = 0.61$) between D_T (μm) and I_M (l^{-1}) for the new data for small polar maritime cumuliform clouds presented in this paper (circles in Fig. 3) is

$$I_M = \left(\frac{D_T}{12.5}\right)^{4.5}. \tag{2}$$

Cloud-top temperatures and maximum ice particle concentrations were uncorrelated ($r = 0.02$) for this same data-set. The measurements in shallow cumulus and stratocumulus clouds obtained on 3 February 1989 (the squares in Figs. 2(d) and 3) provide a particularly good example of how the breadth of the droplet spectrum is better related to maximum ice particle concentrations than is cloud-top temperature. These clouds were sampled about 50–100 km offshore from Vancouver Island in strong, and exceptionally cold, offshore flow. Cloud-base temperature ranged from -16.5 to $-18.0\,°C$ at 85 kPa and cloud-top temperature from -19 to $-24.5\,°C$ (the lowest cloud-top temperature measured in this study). In spite of the low cloud-top temperature on this day, the highest ice particle concentration found in a 250 m path in several hours of flying in 'broken' cloud coverage was only 4.8 per litre (one of the lowest maxima for a cloud with

such a cold top that we have measured). At the same time, the cloud droplets found in the upper portions of these clouds were quite small and led to a D_T value of only 17 μm. These $I_M - D_T$ values for this cloud fit closely the best-fit relationship given as Eq. (3) by HR.

In sharp contrast to clouds with appreciable width, much less ice was found in the narrow ($D < 3$ km), short-lived, 'chimney-type' clouds with subsiding tops (the open circles in Figs. 2(d) and 3) even when D_T was large (>30 μm diameter). This finding agrees with that of Mossop *et al.* (1970, 1972). For some perspective on how small these 'chimney-type' clouds are, it is worth pointing out that in a 10 m s^{-1} wind even the largest of these clouds would require less than 5 minutes to pass over a point on the ground.

(*d*) *Locations of the origins of the ice particles*

Hobbs and Rangno (1985) noted that in the cold, maritime, cumuliform clouds they studied, ice was first detected in localized regions near the cloud top, and the first ice out of the bottom of the cloud was graupel, in filaments a few to tens of metres wide. Also the cloud tops (visually) glaciated within ~5–7 minutes of a turret reaching its maximum height. This was also observed for the wider ($\gtrsim$3 km) clouds in the present study. In fact, near the tops of these clouds ice can form so rapidly and prolifically that it resembles the almost instantaneous formation of ice produced by dry-ice seeding (see section 5(c) below).

Since ice-crystal habits are temperature and humidity dependent, information on the regions of a cloud where ice crystals originate can be surmised from their habits. This is particularly true of small (<400 μm diameter) crystals with relatively short growth histories and low fallspeeds that develop in a water-saturated environment. If a crystal with a well-defined habit is found in a region of a cloud that is more than 1 degC removed from the temperature zone where crystals of that habit grow from the vapour phase, as defined by Magono and Lee (1966) for water-saturated conditions, we say that the crystal was encountered outside of its temperature zone. Only about 4% of the crystals identified on the PSM 2-D imagery, and on the slide replicas, were collected at temperatures colder than that of their temperature zone. Thus, very few of the ice crystals that were intercepted along the flight paths were transported to that region from below. Instead, most of the ice crystals appeared to form *in situ*, or originated at levels above the aircraft flight level. This suggests that, in most cases, ice forms in these clouds when the updraught has nearly halted and the flow is quasi-horizontal or downward.

(*e*) *Radar echo widths*

Figure 4 shows a plot of the frequency of occurrences of various echo widths measured with the 35 GHz radar when it was pointed downward and the aircraft was flying horizontally in or above the clouds. Radar echoes $\lesssim$1 km wide were rare, indicating that it is generally necessary to have a cloud at least 1 km wide to produce a radar echo. However, in most (~95%) clouds that had top temperatures ≤ -7 °C, either a radar echo or drizzle-sized ($\gtrsim$100–400 μm diameter) drops were detected. Thus, these shallow, cold, maritime, cumuliform clouds were very efficient producers of precipitation-sized particles.

5. Two contrasting examples of ice formation in maritime cumuliform clouds

Two quite different ice-forming behaviours were observed in these maritime cumuliform clouds. The first was prolific ice formation in clouds with $D \gtrsim 3$ km. The second was that associated with narrow ($D < 3$ km), 'chimney-type', clouds, which sent one or

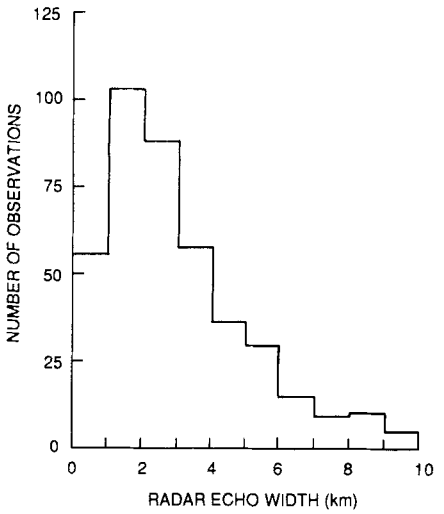

Figure 4. Frequency of occurrence of radar echo widths observed within 1km categories in maritime cumuliform clouds with the downward-pointed 35 GHz radar.

two turrets upwards followed by the rapid collapse of the turrets and often accompanied by evaporation of the cloud base upwards. Relatively few ice particles were found in the 'chimney-type' clouds, although their cloud tops were often relatively cold ($\leq -7\,°C$).

The two types of cloud are initially quite similar in microstructure, but about halfway through their development their structures diverge. As the tops of the 'chimney-type' clouds age and decline, there is a rather sudden onset of drop coalescences that leads to the formation of drizzle drops in concentrations of a few per litre and sometimes as high as ~30 per litre. By this time a few of the drops have frozen. By contrast, as the tops of the wider clouds age, a prolific ice-forming process is activated that interferes with the formation of drizzle drops in high concentrations; instead, high concentrations of vapour-grown ice crystals appear as some of the drizzle drops freeze. In this critical stage, rarely noticed because of its ephemeral nature, drizzle drops, frozen drizzle drops, and high concentrations of tiny ($<300\,\mu m$ in maximum dimensions) ice particles are found.

The different behaviours of these two types of cloud are illustrated in detail by the two case-studies described below.

(*a*) *Low ice particle development in narrow ('chimney-type') maritime cumulus congestus cloud*

A narrow, short-lived, maritime cumulus congestus cloud that was sampled on 3 May 1988 was especially interesting because it attained a depth (2 km) and a cloud-top temperature ($-12\,°C$) where we routinely observe high ice particle concentrations (>100 per litre) in maritime cumuliform clouds with $D \gtrsim 3$ km, yet this narrow cloud produced relatively few (<10 per litre) ice particles. Indeed, only a few minutes before this cloud was sampled, we measured ice particle concentrations >200 per litre in the top of a neighbouring isolated maritime cumulonimbus cloud (radar echo ≈4 km wide) that also had a top temperature of $-12\,°C$.

The 'chimney-type' cloud grew rapidly out of a weak line of cumulus humilis and cumulus mediocris clouds a few kilometers off the Washington State coast. An aircraft sounding made in the vicinity of the cloud (Fig. 5) shows that the air was relatively moist from cloud base to cloud top. Cloud bases were at 94 kPa (0.6 km a.s.l.) where the

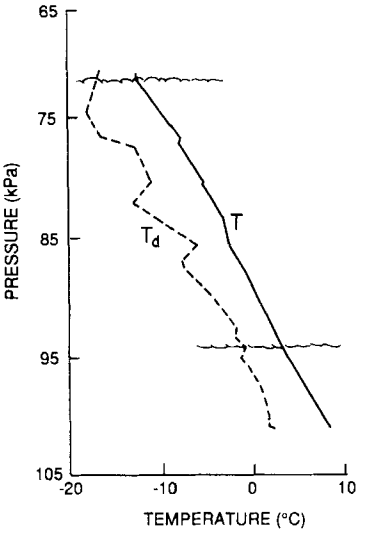

Figure 5. Temperature and dewpoint sounding obtained from the aircraft in and around the cumulus congestus cloud of 3 May 1988. Cloud base and cloud-top heights are indicated by scalloping.

temperature was 3 °C. Six aircraft passes were made through this cloud, between 1401 and 1417 Pacific Standard Time (PST), with the first three passes at or near cloud top.[2]

A summary of some of the measurements is shown in Fig. 6. Cloud droplet concentrations (~115 cm^{-3}) were about 50% higher than the average value for maritime cumulus in this region. The relatively high droplet concentrations were probably due to partial 'continentalization' of maritime air that had moved inland the previous night and then offshore during the morning hours preceding and during the early portions of the flight. Nevertheless, large (>30 μm diameter) droplets in concentrations >1 cm^{-3} were present near the cloud top.

Drizzle-sized (100–400 μm diameter) drops (liquid and frozen) were also present at several levels in the cloud; at one point, when the cloud top was descending rapidly, concentrations of ~10–30 per litre of these drops were measured over a distance of 0.4 km. Vapour-grown ice crystals were extremely rare; only a few were collected on the microscope slides or imaged by the PMS 2-D probes.

The first aircraft pass (at 1401 PST) was at 73 kPa (−11.5 °C) through a hard-looking cumulus turret with a cauliflower appearance (indicative of vigorous updraughts), which was ~2 km above cloud base and ~50 m below cloud top. We estimated, from the aircraft video record, that this cloud had ascended through the −7 °C level about 2–3 minutes prior to the first aircraft pass. Some ice particles were detected by the OIPC (Fig. 6(a), top panel). From the PMS 2-D imagery (Fig. 6(a), bottom panel), and from the video record of particles hitting the aircraft windscreen, these ice particles were seen to consist of frozen, drizzle-sized drops and/or small graupel.

A weak 35 GHz radar echo developed at or near cloud top between the first and second aircraft passes (1401–1404 PST, Fig. 6(a) and 6(b), middle panel). The echo descended rapidly, and its base was near ground level by 1410 PST (Fig. 6(c) and 6(d), middle panel), but it did not strengthen as it approached the ground (presumably because

[2] Interestingly, although the aircraft crossed previous flight tracks in some of these passes, APIPs were not detected. Thus, this cloud appeared to be resistant not only to the formation of natural crystals but also to those produced by aircraft.

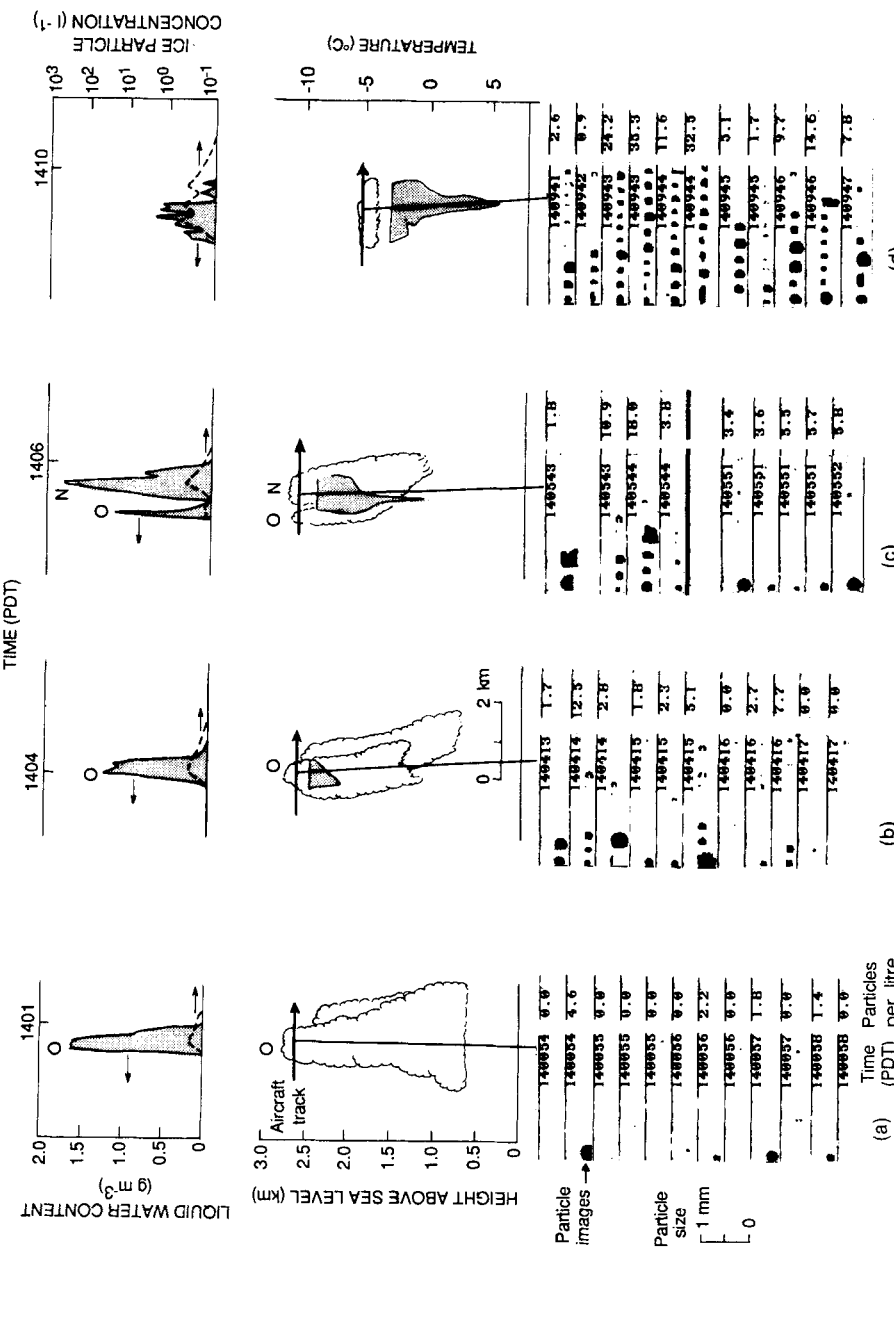

Figure 6. Some measurements obtained in the first four passes (a–d) through a small maritime cumulus congestus cloud on 3 May 1988. Top panel shows liquid water contents (solid line) and OIPC ice particle concentrations (dashed line). Middle panel indicates echo returns from the 35 GHz radar; light shading indicates minimum detectable echo and dark shading two echo intensity categories higher. Flight level is indicated by a heavy arrowed line. Scalloping denotes approximate boundary of the cloud as determined from video camera and other photographic records. Lower panel shows samples of the PMS 2-D imagery for cloud particles and particle concentrations along the flight track at the times indicated. Scale for the cloud particles is shown on left-hand side of lower panel.

the precipitation partially evaporated in the dry air into which the cloud top was collapsing).

The cloud had changed noticeably in texture by the time of the second aircraft pass, which took place at the same level, from the same side of the cloud, and at the same height as the first pass, but 3 minutes later. The turret now appeared softer and frayed at the edges as the cloud top began to decline and evaporate while shearing away from the lower part of the cloud. The peak liquid water content had declined from ~1.6 to 1.2 g m^{-3} (Fig. 6(a) and 6(b), top panels), and the concentration of drizzle-sized drops (frozen or liquid) increased to a few per litre (Fig. 6(b), bottom panel). Several snowflakes or graupel particles struck the aircraft windscreen, but, owing to their very low concentrations, none of these were imaged by the PMS 2-D cloud or precipitation probes. Several hexagonal plates, ranging from ~10–70 μm diameter, were collected on a slide exposed during this pass.

A third pass was made at cloud top from ~1405–1406 PST. The original turret sampled was now descending rapidly, but a slim and firm-looking turret, which had just arrived at flight level was also sampled. The composition of the firm-looking turret was virtually identical to that of the original turret when it was first sampled but it contained even more liquid water (1.8 g m^{-3}, Fig. 6(c), top panel, marked N). A slide was exposed in the firm-looking turret but only droplets were replicated. Meanwhile, the liquid water content in the original turret had declined to 1.2 g m^{-3} (Fig. 6(c), top panel, marked O). A few ice particles were imaged in this decaying turret by the PMS 2-D cloud probe (Fig. 6(c), bottom panel), but the maximum concentration appears to have been ~10 per litre and consisted almost entirely of frozen drops or graupel-like snow. A burst of snow was seen on the windscreen during this passage. No other turrets ascended to cloud top.

About 4 minutes elapsed between the third and fourth passes through this cloud as the aircraft descended towards the collapsing, frayed and ragged cloud that now comprised both turrets. The fourth aircraft pass was at the upper fringes of the descending cloud top (at 80 kPa and at −5.6 °C), which was about 5 degC warmer than for the previous pass. The liquid water content in this pass continued its decline to 0.8 g m^{-3} (Fig. 6(d), top panel). Drizzle-sized drops, liquid and frozen, with some vapour-grown ice crystals were seen in the PMS 2-D imagery; the combined peak concentrations were ~10–30 per litre (Fig. 6(d), bottom panel). Some of the drops encountered on this fourth pass were frozen, as indicated by spikes in the OIPC (Fig. 6(d), top panel) and from the video record by the opacity of some of the drops when striking the windscreen. However, the build-up of ice on the windscreen showed that many (probably most) of the drops were not frozen. The OIPC indicated that maximum ice particle concentrations were 2 per litre. Only liquid or frozen droplets, no vapour-grown crystals, were replicated on a microscope slide exposed during a portion of this pass. Visually, there was no sign of ice in the form of fallstreaks or fibrous structure. It is likely, however, that the concentrations of drizzle-sized particles (liquid and frozen) present below the flight level were greater than 2 per litre, particularly in view of the long fallstreak seen in the radar record (Fig. 6(c) and 6(d), middle panel).

The fifth aircraft pass (at 1413 PST and at 86 kPa and −2.2 °C) was flown in some remaining shreds of cloud that comprised the original two turrets. Apparently the strongest radar echo was either missed or disappeared, since the downward-pointing 35 GHz radar did not record any echoes. However, a few drizzle-sized drops were imaged by the PMS 2-D probes; they consisted of liquid or frozen drops and several ice columns <300 μm in length. The total concentration of these particles was less than 1 per litre. At this time, the cloud was stratiform in appearance, ragged, and no longer descending. The liquid water content was less than 0.1 g m^{-3}.

The last pass (at 1417 PST) was underneath the remnants of this cloud. A few raindrops spattered on the windscreen in concentrations ≤ 0.2 per litre. There was no radar echo.

(*b*) *Formation of high ice particle concentrations in a small maritime cumulonimbus capillatus cloud*

On 21 November 1988 we studied three relatively isolated cumulonimbus clouds that formed in post-frontal convection off the Pacific coast of Washington State in a west to south-west airflow with a trajectory of several thousand kilometers over water. The air was quite moist through 85 kPa (−6 °C), with a dry layer above (Fig. 7). Strong vertical speed shear caused the upper portion of the clouds to shear off toward the north-east. Cloud bases were at 94 kPa (6 °C). The air below cloud bases was more turbid than usual due to a whitish haze with horizontal visibility in the sub-cloud layer estimated at <15 km. Droplet concentrations were low ($\approx 65\,cm^{-3}$).

Three clouds were studied on this day. The first was a cumulus congestus cloud with $D = 3.1$ km and a top between −6 and −7 °C. Maximum ice particle concentrations, which were encountered in the oldest portions of the cloud on its downwind side, were 1–5 per litre. The ice was frozen drops and small graupel. The second and third clouds were larger, $D = 6.5$ and 7 km, respectively, with tops at −9 and −12 °C, and maximum ice particle concentrations of ~250 and ~340 per litre, respectively. In the regions of these two clouds where the highest ice particles concentrations were measured, the crystals were largely columnar. All of these clouds had droplets >30 μm diameter in concentrations $>1\,cm^{-3}$ at cloud top. Drizzle-drops, in maximum concentrations of a few to 30 per litre, were also present near cloud tops.

Since the third cloud behaved similarly to many other highly ice-producing maritime clouds with $D \geq 3$ km that we have sampled, including the second cloud on this day, we

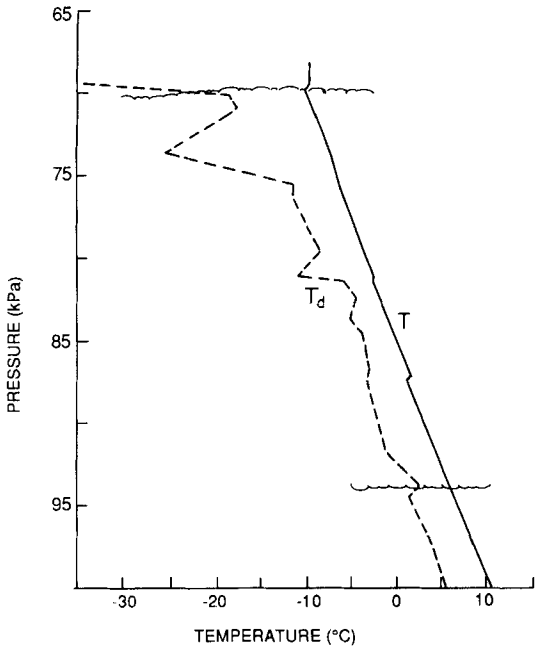

Figure 7. Temperature and dewpoint sounding obtained from the aircraft in and around a maritime cumulonimbus capillatus cloud on 21 November 1988. Cloud base and cloud-top heights are indicated by scalloping.

will describe in some detail the measurements and observations for this cloud. This cloud resembled that indicated by A in Fig. 1. The third cloud was particularly interesting because: (i) it spanned five ice-crystal habit temperature zones (needles, sheaths, columns, plates, and sector plates), (ii) it was isolated with maximum and minimum horizontal dimensions of ~1.5 km and ~7 km, (iii) its cloud top did not descend rapidly after reaching its maximum height, (iv) its top extended well into a dry layer that overlay the marine boundary layer, thus allowing maximum effects due to evaporation, and (v) it had a large degree of vertical lean, so that much of the graupel and other ice particles that formed near cloud top were carried away from droplet regions in the rising portions of the cloud upwind.

Prior to penetrating this cloud, the aircraft was flown at −9 °C, above building cloud tops. On ten occasions, the aircraft flew over segments of the cloud in which *in situ* measurements were subsequently obtained. No radar echoes were detected below the flight level during the period (1341–1348 PST) of the overflight. As noted before, if ice particles with maximum dimensions $\gtrsim 100\,\mu$m had been present in concentrations $\gtrsim 1$ per litre (or millimetre-sized graupel present in concentrations $\gtrsim 0.1$ per litre) the radar would have detected an echo. The first aircraft penetration of the cloud, which occurred ~8 minutes after an overflight of the cloud, was just below cloud top (which had now risen to the −10 to −11 °C level). Ice particles were measured in peak concentrations >100 per litre and the cloud was now producing a radar echo. Hence, near the tops of this cloud, ice particles ~100 μm in maximum dimensions must have increased in concentrations from <1 per litre to >100 per litre in only 8 minutes.

Five aircraft passes were made through the cloud, each at successively lower levels, with the first at cloud top and the last at cloud base. Each pass was 0.3–0.6 km lower than the previous pass. Sampling was between 1352 and 1419 PST. The cloud was fed by air from the up-shear side, where the cloud had a firm cauliflower appearance (Fig. 8(a)). The building, up-shear (western) region of the cloud was virtually ice-free to at least the −7 °C level, but ice particle concentrations >100 per litre were encountered in localized (<20 m) regions in the top of the first turret. Because of the pronounced inclination of the cloud, most of the crystals that formed in the summits of the two turrets fell out through air that contained ice particles rather than liquid water. The western portion of the cloud consisted mainly of supercooled droplets, but it also contained some graupel in a narrow zone.

The first pass was from the down-shear to up-shear portion of the cloud and through the top of the two tallest turrets. The first turret (marked A in Fig. 8) was selected because it had reached its maximum height, was beginning to decline, and was seen to be composed mainly of ice. The second turret (B in Fig. 8) was closer to the up-shear side of the cloud and in an earlier stage of its life cycle. The minimum temperatures measured in the two turrets were −10.0 and −10.9 °C, respectively; liquid water contents peaked at 0.3 and 0.7 g m^{-3}, respectively (Fig. 8, top panel). The maximum ice particle concentrations encountered were >100 per litre (Fig. 8, bottom panel). The ice particles in the first and older turret consisted of plates, sector plates (about 60%), and hollow columns (about 40%). Plates and sector plates form at temperatures between −10 and −13 °C, and hollow columns between −8 and −10 °C (Magono and Lee 1966). Nearly all of these ice particles were small (<500 μm in maximum dimension) and vapour-grown (Fig. 8, bottom panel, and Fig. 9). Diffusional growth-rate calculations for a water-saturated environment show that the slower growing, plate-like crystals must have formed <13 minutes before they were intercepted.

The ice particles in the second turret were quite different from those in the first. These ice particles were small and in lower concentrations (~10 l^{-1}); they consisted

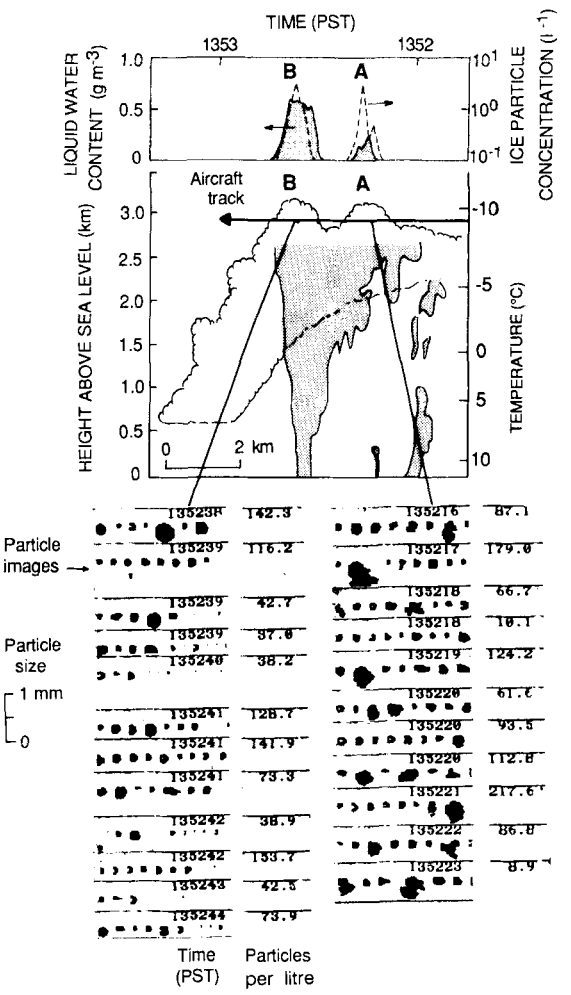

Figure 8. As for Fig. 6 but for the first aircraft pass from the down-shear to the up-shear portion of a small isolated maritime cumulonimbus capillatus cloud on 21 November 1988.

largely of frozen drops and small graupel with few vapour-grown crystals (Fig. 8, bottom left panel). This up-shear/upwind turret was in the initial stage of ice formation when we intercepted it. There was no indication that ice particles were being advected to cloud top from below, since columnar crystals were not observed. Rather, the ice was apparently forming *in situ* as drops ($<400\,\mu$m diameter) froze. Nevertheless, many (maybe most) of the drops in this turret were supercooled liquid, since a heavy coating of ice formed on the aircraft windscreen.

The 35 GHz radar echoes from the clouds beneath the first pass (Fig. 8, middle panel) shows that precipitation was not reaching the ground directly under turret A, but that it was beneath the second turret (B). Hence, while ice was relatively new in the top of the second turret, precipitation had already reached the ground directly below it. Precipitation from the first turret A extended ~1.5 km below flight level; it was part of a contiguous region of precipitation, the lower portions of which sloped downwards toward the surface from the older turret A (from which ice particles fell out in clear air) to the newer turret B (Fig. 8, middle panel).

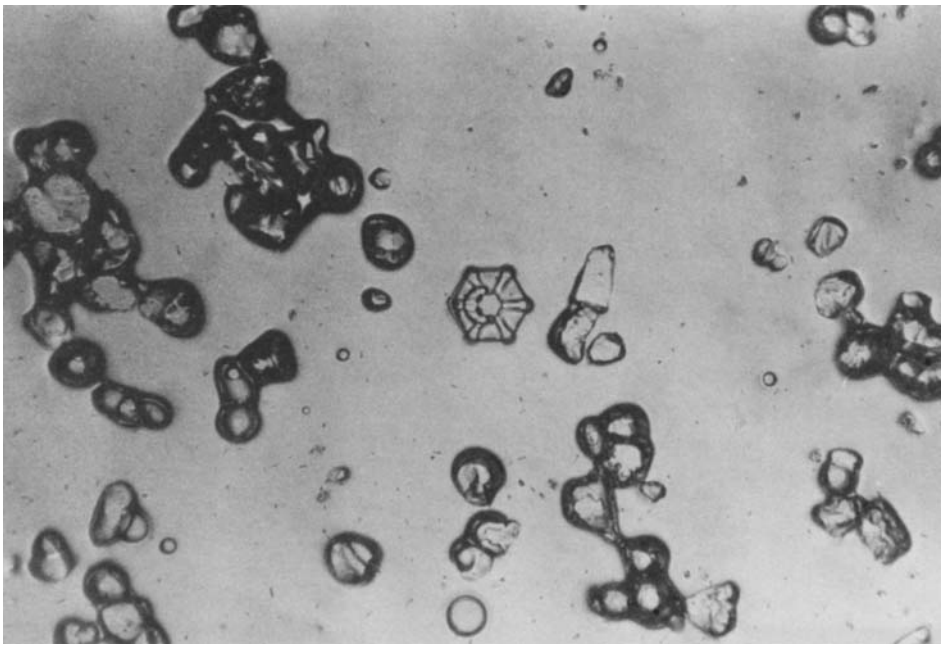

Figure 9. Crystal replicas obtained in an aging turret of a small isolated maritime cumulonimbus capillatus cloud top at 1352 PST on 21 November 1988. The temperature at the top of the turret was −10 °C.

The second pass through this cloud (at 1357 PST, 75 kPa and −7 °C), which again began at the down-shear/downwind portion of the cloud, was through the heart of the 'plume' of ice particles. The observations for this pass are shown in Fig. 10. The downward-pointing 35 GHz radar return (Fig. 10, middle panel) shows that initially some of the cloud and precipitation was below this horizontal flight leg. As the aircraft flew upwind, precipitation trails lengthened progressively below flight level, until they reached the ground near the mid-point of the cloud. Up to and including the point where the precipitation reached the ground, the cloud consisted almost entirely of ice composed of columnar crystals, quasi-spherical particles, and aggregates (Fig. 10, lower panel). Maximum ice particle concentrations in the second pass peaked at 290 per litre over a 250 m path length, with a highest 1 km average of 250 per litre. These peak concentrations were produced mainly by hollow columns (Fig. 11), although other adjacent cloud regions contained 50–100 l^{-1} of non-columnar crystals (e.g., Fig. 10, bottom right panel) that had descended from above. Since hollow columns form between −8 and −10 °C, these crystals must have grown *in situ* or just above the flight level.

A sharp transition to a mainly liquid water cloud occurred as two newly risen turrets were encountered on the up-shear (western) end of this narrow, but long cloud. These two turrets were situated above and just upwind of the location where the precipitation first reached the ground. The first turret (labelled C in Fig. 10, top panel) contained ice particle concentrations of 10–30 per litre. These ice particles consisted of graupel-like particles (of which <1 per litre were millimetre-sized), and columnar crystals <400 μm long (Fig. 10, bottom left-centre panel). The liquid water content peaked at ~0.7 g m^{-3} (Fig. 10, top panel). The second turret (labelled D in Fig. 10, top panel) was young and its top was not much above the flight level. It was virtually ice-free, but contained a few frozen drops (Fig. 10, top and bottom left panel). A 35 GHz radar echo extended just

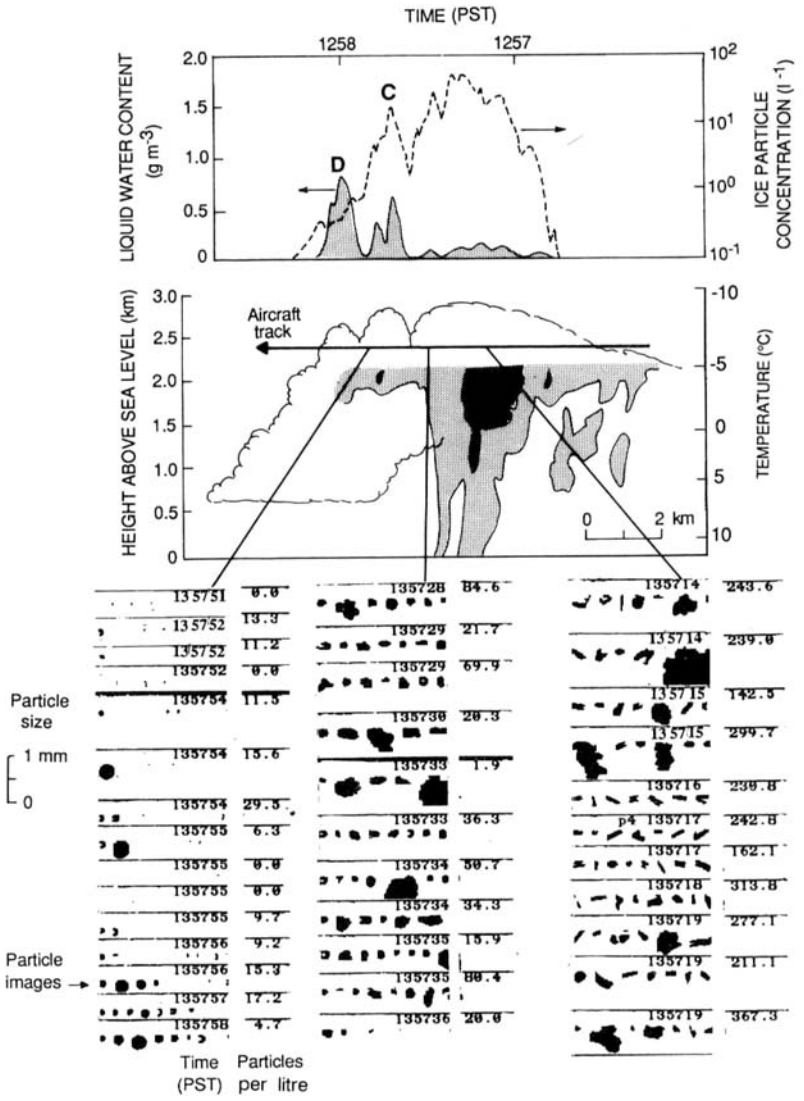

Figure 10. As for Fig. 6 but for the second aircraft pass from the down-shear to the up-shear portion of a small isolated maritime cumulonimbus capillatus cloud on 21 November 1988.

below flight level in each of these turrets (Fig. 10, middle panel) indicating that the precipitation encountered in turret D had arrived at the flight level within the previous few minutes.

The third pass through this cloud, which began at 1400 PST, was from the up-shear to down-shear portions of the cloud (Fig. 12). The aircraft entered the most vigorously rising, and firmest looking, portion of this cloud. The pass was at 77.5 kPA, between −4.5 and −5.5 °C, or about 0.3 km lower than the previous pass. The peak liquid water content, encountered on cloud entry, was 1.7 g m^{-3}, or about twice that recorded on the second pass.

Five distinct microstructural regions were observed in the third pass. They were, in the order encountered: (i) an ice-free, high liquid water region, (ii) a region of high liquid water that contained a few graupel particles, (iii) a region containing columnar

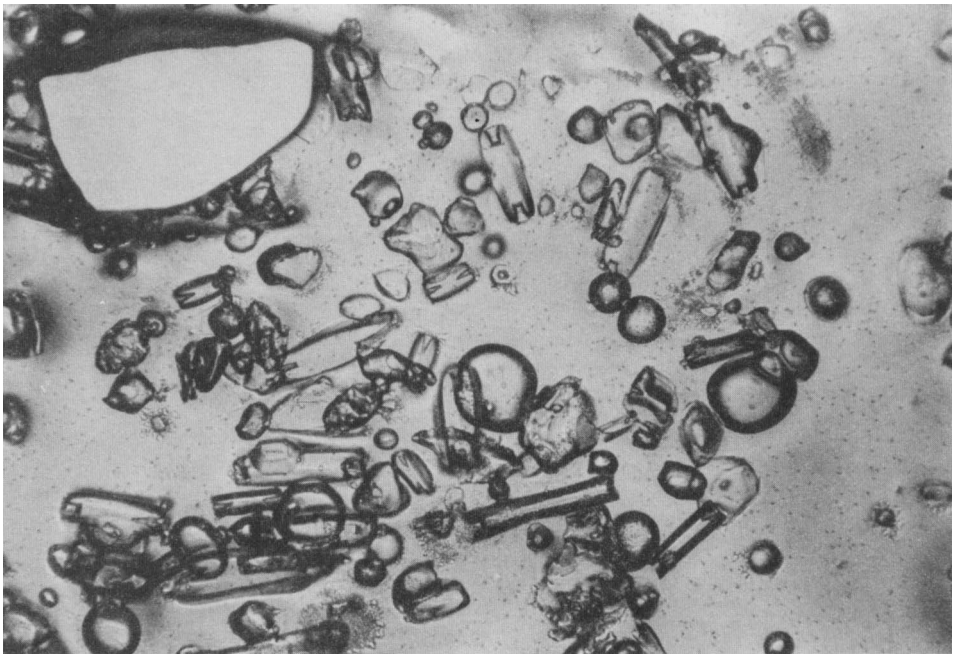

Figure 11. Crystal replicas obtained in a small isolated maritime cumulonimbus capillatus cloud at 1357 PST on 21 November 1988.

crystals (where the highest ice particle concentrations were measured), (iv) a region containing plate-like crystals, and (v) a region containing mostly large aggregates of columnar crystals. The last three regions were virtually free of any liquid water.

The first region, which occupied the first kilometre of the pass, consisted almost entirely of cloud droplets; no ice particles were detected (Fig. 12, top and bottom left panel). Owing to the tilt of the cloud top (Fig. 12, middle panel), this portion of the pass was underneath the warmest portion of the cloud top. Although one or two drizzle-sized drops were encountered in this region, no precipitation was detected by the 35 GHz radar (Fig. 12, middle panel). This may have been due to the low concentration of the drops, or because they had not descended far enough below the flight level (about 250 m) to be detected by the radar.

The second distinct microstructural region was about 0.8 km wide; cloud droplets, several graupel particles, and an occasional drizzle drop were encountered in this region (Fig. 12, bottom left-centre panel). The PMS 2-D precipitation probe imagery (which has a much larger sampling volume than the 2-D cloud probe, and therefore provides more reliable measurements of particles present in low concentrations) showed that the average concentration of millimetre-sized graupel across the 0.8 km leg was only 0.12 per litre. Nevertheless, precipitation reached the surface under this region of the cloud and the radar echo was strong (Fig. 12, middle panel), which suggests that larger particles were present below the aircraft. The strongest portion of the echo, which extended 1.5 km below the flight level, was located below the point where the graupel particles were encountered. With an assumed graupel fall speed of 2–4 $m\,s^{-1}$, graupel or other larger particles would have fallen through the flight level only about 7–4 minutes earlier.

The third distinct microstructural region, which was about 2.5 km long, contained a few large ice particles but extremely high (at times >400 per litre) concentrations of

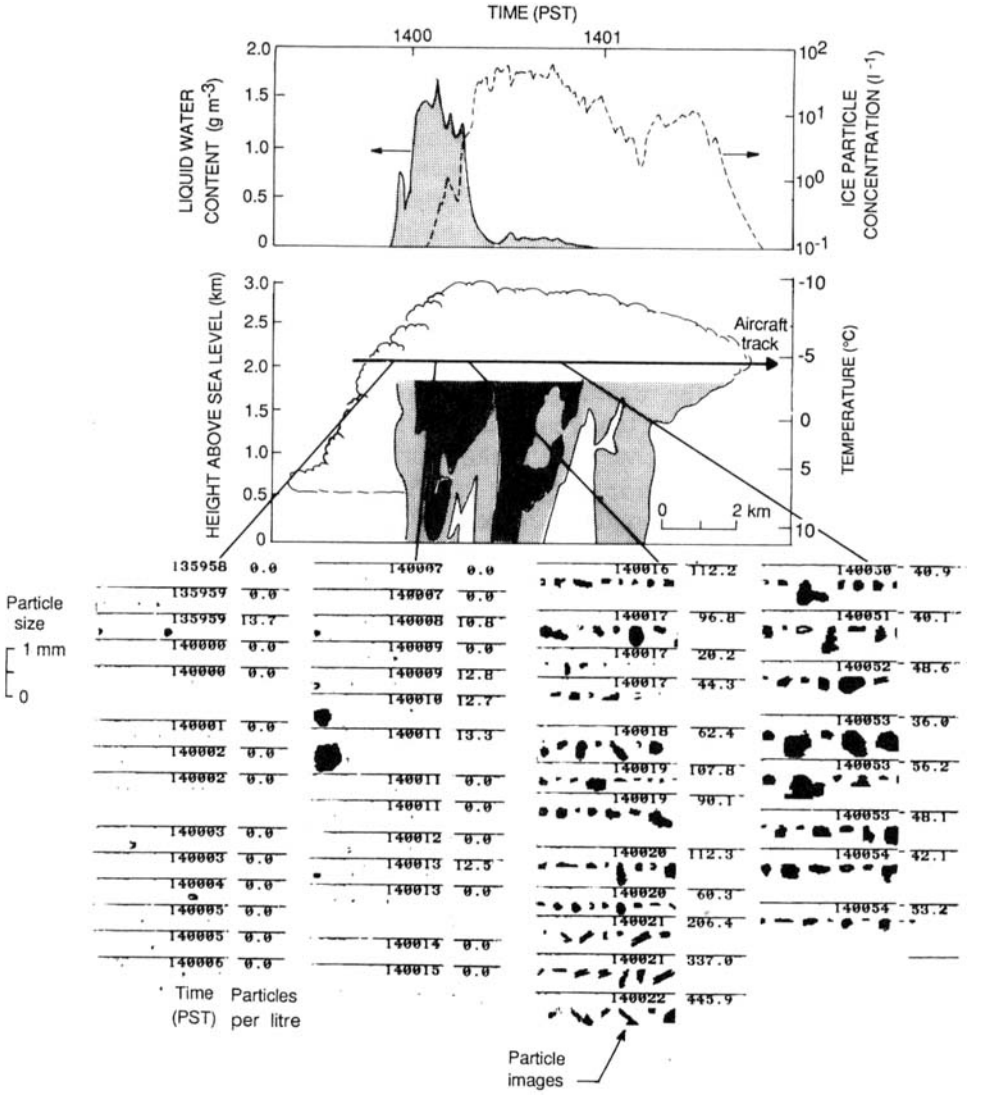

Figure 12. As for Fig. 6 but for the third aircraft pass, from the down-shear to the up-shear portion of a small isolated maritime cumulonimbus cloud on 21 November 1988.

single columnar crystals with maximum 250 m and 1 km concentrations of 340 and 290 per litre, respectively. More than 90% of the columnar crystals in this region were $< 600\,\mu$m in maximum dimension (Fig. 12, bottom centre panel), indicating that they had formed about 8 minutes earlier. Increases in ice particle concentrations from near zero to >100 per litre over horizontal distances of 40–50 m, and from near zero to >300 per litre over 300–500 m, were observed as the aircraft few down-shear. (Recall that several overflights of this portion of cloud approximately 12 minutes earlier had not disclosed an echo, therefore, at this time the concentrations of ice particles with maximum dimensions $\gtrsim 100\,\mu$m were less than 1 per litre.) The interception of the high ice particle concentrations virtually marked the end of liquid water (Fig. 12, top panel) for the remainder of this pass. The 35 GHz radar returns during the in-cloud pass showed two segments of

strong returns that reached the ground (Fig. 12, middle panel). Both were associated with higher concentrations of millimetre-sized aggregates of columnar crystals.

The fourth distinct region, which was entered at 140048 PST, was about 2 km wide. The maximum 1 km ice particle concentration was 50 per litre, with localized concentrations >100 per litre. These consisted of amorphous and quasi-spherical particles (Fig. 12, bottom right panel); they may have been rimed, single plates or aggregates of plate-like crystals. These particles must have originated at cloud top, where the temperature (−10 to −12 °C) was appropriate for the growth of plates. There was no liquid water in this region—further indication that this was an older, debris-type cloud that had descended from a higher level. Also, the ice particle concentrations found here were similar to those found at cloud top in the first aircraft pass.

Finally, a region about 2 km long, containing single and aggregates of columnar crystals, but no liquid water, was encountered. Total ice particle concentrations were ~10 per litre. The crystal habit (columns), and the location of this region at the outflow end of the cloud, suggests that we were in the debris of a turret that had a top warmer than −9 °C. Light precipitation reached the ground under this region (Fig. 12, middle panel). The concentrations of millimetre-sized ice aggregates present here were slightly higher compared with what had been found in the previous microstructural region.

The fourth pass was at 82.5 kPa (−1.9 °C) and was from the down-shear, glaciated side to the up-shear side of the cloud. These measurements (not shown) resemble the sequence described for the preceding pass, except that ice particle concentrations, because of growth and aggregation as they settled to this level, were lower and the ice particles were larger.

To summarize, based on radar measurements during the overflight of this cloud and subsequent *in situ* measurements, we have deduced that the concentrations of ice particles just below cloud top (−10 and −11 °C) increased from <1 to >100 per litre in ~8 minutes. From the sizes of the ice crystals measured near the tops of these clouds we have deduced from diffusional growth calculations that ice particles in concentrations >100 per litre formed within 8–13 minutes. Since these crystals were relatively small, and the majority were plates, they must have originated near cloud top. Subsequently, similar concentrations of ice plates were observed on the downwind portion of the cloud from cloud top to near cloud base. Between −7 and −4 °C, small columnar ice crystals in concentrations >200 per litre also formed very quickly *in situ*. The average concentration of millimetre-sized graupel adjacent to and upwind of this region was only 0.16 per litre. The average graupel concentration in the region of high ice particle concentrations was 0.80 per litre, although there was little liquid water.

The above account provides a general description of the evolution of ice commonly observed in more than one hundred wider ($D \gtrsim 3$ km) polar maritime cumuliform clouds that we have studied.

(*c*) *Comparisons with the development of ice particle concentrations produced by dry-ice seeding of a small cumulus cloud*

To emphasize how rapidly high concentrations of ice particles appeared in the natural, maritime cumuliform clouds described in subsection (*b*) above, we will now compare them with ice particles produced artificially by seeding similarly sized, continental-type cumiliform clouds with dry ice. The advantage of comparing a seeded cloud with a natural cloud is that in the former case all of the ice particles form at approximately the same (known) time. Thus, if the high concentrations of natural ice particles in maritime clouds form very quickly and in localized regions, they should be similar in appearance to those formed by localized dry-ice seeding.

On 1 February 1979 a 'continental-type', cumlulus mediocris cloud developed in cool air flowing offshore over the Washington State's coastal waters. Cloud top and base temperatures were −5.8 °C and 2.5 °C, respectively. This cloud contained copious ($>2\,g\,m^{-3}$) liquid water and no natural ice particles. The maximum concentration of natural ice particles observed in any cumulus cloud on this day was 0.1 per litre (see Table 1 of HR). The cloud was in its maximum 'bulging' stage when it was seeded for about 30 seconds with dry ice at a rate of $0.8\,kg\,km^{-1}$ over a distance of ~3.6 km. Figure 13 shows the microstructural record for this cloud during the 16 minutes following seeding. During this period, nine aircraft passes were made through the cloud at about 2-minute intervals.

The OIPC record and the PMS 2-D cloud-probe imagery show that no ice particles were detected and the liquid water content was $>2\,g\,m^{-3}$ in the first pass (Fig. 13(a), top and bottom panels).

On the second pass (at 1533 PST and 120 seconds after seeding) a small but sharp response was observed on the OIPC (Fig. 13(b), top panel). Numerous tiny, quasi-spherical particles, presumed to be embryo ice crystals ($<100\,\mu m$ diameter), were simultaneously imaged by the PMS 2-D cloud probe (Fig. 13(b), bottom panel). Such 2-D images, encountered in the heart of a young dry-ice plume, have not been seen in natural clouds. Cloud particles collected on microscope slides taken in other young dry-ice plumes show that these types of PMS 2-D cloud-probe images are produced by very large numbers of small ($<70\,\mu m$ in maximum dimension) unrimed, pristine ice particles. However, all of the subsequent 2-D images seen in dry-ice plumes (as described below) look like the imagery from natural (unseeded) maritime clouds that pass through a prolific ice-forming stage (see section 5(b)).

On the fourth pass through this cloud, and $5\frac{1}{2}$ minutes after seeding, high (>300 per litre) ice particle concentrations were intercepted, with peak concentrations >1000 per litre (Fig. 13(c), top and bottom panels). The ice particles were columnar with small ($<400\,\mu m$ diameter) ice aggregates also present. The liquid water content had diminished by this time to a peak value of $1.4\,g\,m^{-3}$ at the edge of the dry-ice plume. The longest columnar crystals were just approaching dimensions of $50\,\mu m \times 300\,\mu m$ (Fig. 14(c), bottom panel), which is near the size to be expected after about 5 minutes of diffusional growth in a water-saturated environment.

The PMS 2-D imagery recorded on this pass through a young dry-ice plume cannot be distinguished from the imagery encountered in (unseeded) polar maritime cumiliform clouds following the onset of a prolific natural ice-forming stage. In the latter clouds, the prolific ice-forming stage appears nearly coincident with, but just after, the freezing of some larger drops while the cloud top is rising slowly or holding altitude. Compare, for example, the 2-D imagery of the ice particles in the young dry-ice plume in Fig. 13(c) (bottom panel) with that shown in Figs. 10 and 12 (bottom panels) for ice particles encountered in a small (unseeded) maritime cumulonimbus cloud. Perhaps the most remarkable observation is that the peak concentration of ice in natural clouds immediately following the onset of the prolific ice-forming stage can be as much as 50% of the ice particle concentrations measured in dry-ice plumes at a similar instant (see also Hobbs and Rangno 1990).

Aggregation was well under way by the time of the fifth pass through the dry-ice seeded cloud, which was 7 minutes after seeding at ~1538–1539 PST (Fig. 13(d), bottom panel). The maximum 1 km ice particle concentration was 640 per litre, with peaks at times >1000 per litre. The largest dimensions of the columnar crystals had increased to about $70\,\mu m \times 400\,\mu m$ (Fig. 13(e), bottom panel) in water-saturated regions. Maximum liquid water content had decreased to $\sim 0.4\,g\,m^{-3}$.

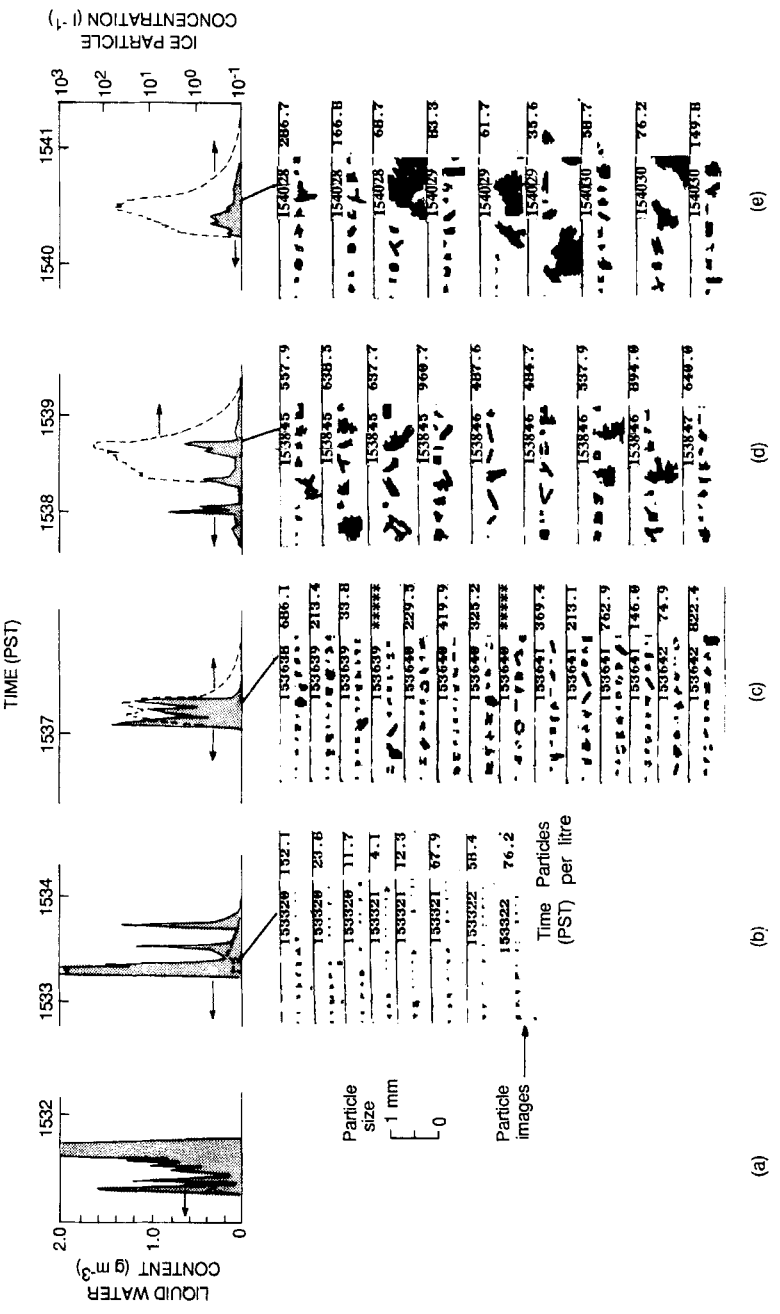

Figure 13. As for Fig. 6 (without middle panel), but for a continental-type cumulus mediocris cloud seeded with dry ice on 1 February 1979.

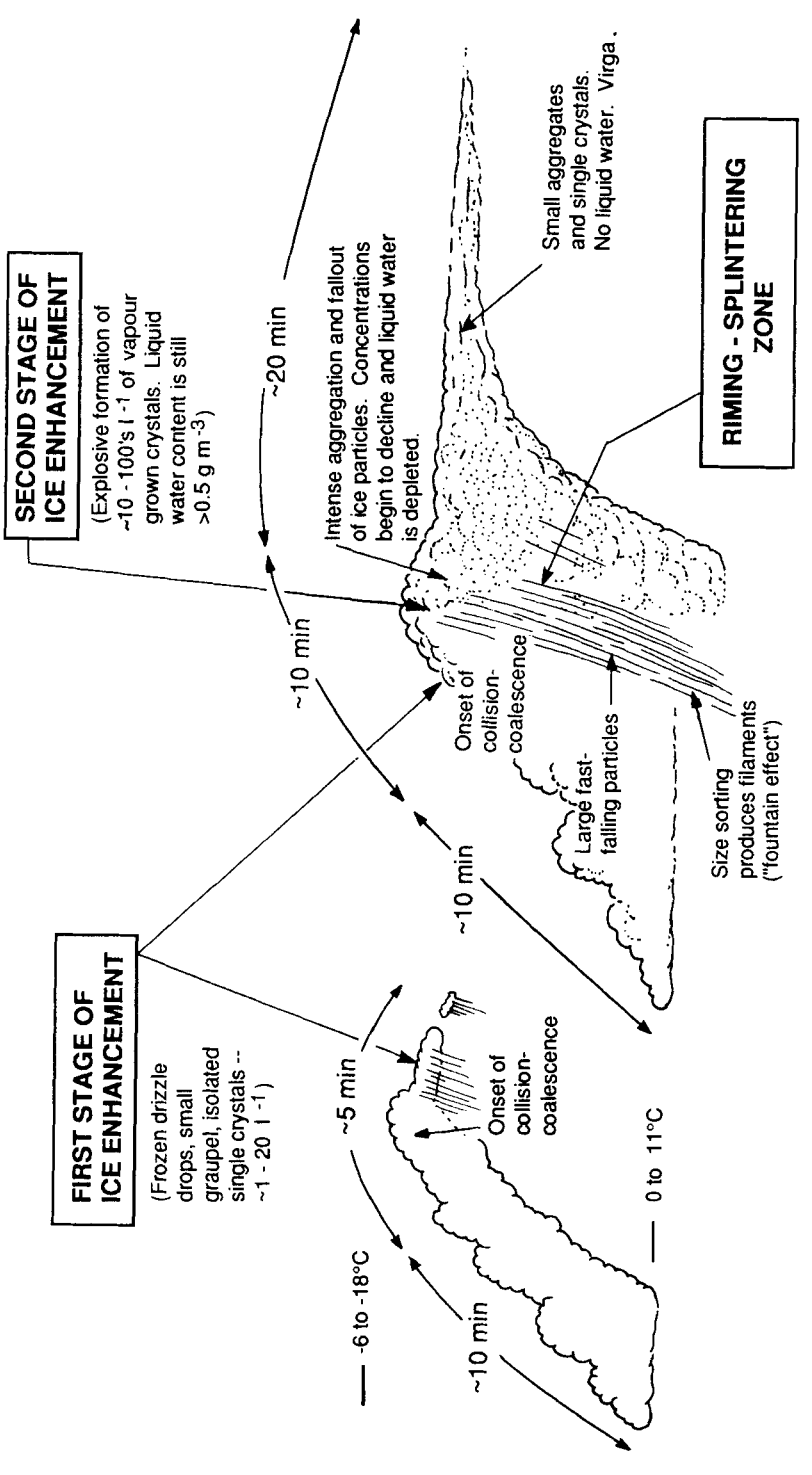

Figure 14. Schematic of observations and speculations presented in this paper on the formation of high ice particle concentrations in small polar maritime cumuliform clouds. The clouds on the right and left represent those indicated by A and B in Fig. 1.

Ice particle concentrations and liquid water contents steadily diminished during the next four passes through the seeded cloud as more ice aggregates formed (e.g., Fig. 13(e) and (f), bottom panel). Peak 1 km ice particle concentrations of 345, 340, 310 and 125 per litre, respectively, were recorded in these four passes. At 9 and 11 minutes after seeding, the largest columnar dimensions were about 80 μm × 500 μm and about 100 μm × 700 μm, respectively, in limited water-saturated regions. Many more crystals, however, were stunted in growth and did not reach these sizes. The concentration of 125 per litre was measured 15 minutes after seeding. By the time of this last pass through the seeded cloud, the maximum liquid water content had diminished to 0.2 g m^{-3}.

In this artificially seeded cloud, the rise and decline in ice particle concentrations, and the appearance of the ice crystals in the 2-D imagery, mimic very closely the evolution of the ice particles from the up-shear/upwind to down-shear/downwind regions in the small, natural, maritime cumulonimbus cloud discussed in section 5 (b) (see Fig. 1). Compare, for example, Fig. 12 (bottom panel) with Fig. 13(d-e) (bottom panel).

6. Evaluation of some possible ice enhancement processes

In this section we make use of the observations described above to evaluate some of the processes that have been proposed to explain the formation of high ice particle concentrations in clouds. Our main findings concerning the development of high ice particle concentrations in polar maritime cumuliform clouds, which should be explained by a satisfactory theory, are as follows:

(i) The first stage in ice formation involves the freezing of drizzle drops (≈100–400 μm diameter) in concentrations of a few per litre near cloud top.

(ii) In the highly ice-producing clouds, with widths ≳3 km and top temperatures between −6 and −18 °C, the second ice-forming stage is characterized by the very rapid appearance of 10 to 100 per litre of small, pristine, and largely vapour-grown, ice crystals that appear to form *in situ* in the middle and upper regions of the cloud. The concentrations of these ice crystals increase by factors of 100–1000 in less than 10 minutes.

(iii) Narrow ($D < 3$ km), 'chimney-type', clouds with subsiding tops do not exhibit the second ice-forming stage. Consequently, ice particle concentrations in these clouds are generally <10 per litre.

(iv) In the highly ice-producing clouds, the second ice-forming stage begins as the collision–coalescence process gets underway, but before or near the time that drizzle drops have reached their maximum concentrations. Owing to the prolific formation of ice, the collision–coalescence process is truncated.

(v) Our new measurements in maritime clouds, and our previous measurements in both maritime and continental clouds (HR), indicate that the tail of the drop size distribution (as measured by the threshold diameter D_T) is a better predictor of the maximum ice particle concentrations that will develop in cumuliform clouds than is cloud-top temperature.

(*a*) *The riming–splintering process*

This process is based on the laboratory measurements of Hallett and Mossop (1974), Mossop and Hallett (1974), Goldsmith *et al.* (1976), and Mossop (1976). The earlier measurements showed that ice splinters are produced when a supercooled cloud at temperatures between −3 and −8 °C, containing ≥1 cm^{-3} of droplets >23 μm diameter, produces riming on an ice surface moving at speeds ≥1.4 m s^{-1}. In natural clouds, the

riming ice surface is postulated to be millimetre-sized graupel particles because of their relatively high fall speeds. Later measurements (Goldsmith *et al.* 1976; Mossop 1978; Mossop 1985c) revealed a dependence of ice-splinter production on the concentrations of droplets $\leq 13\,\mu$m diameter as well as the concentration of larger drops. As the concentrations of these smaller droplets decreased, so did the numbers of ice splinters produced for a given concentration of droplets $>23\,\mu$m diameter and a given velocity of the riming surface.

Observations of the small cumulonimbus cloud on 21 November 1988, and the narrow, 'chimney-type', cumulus cloud on 3 May 1988, described in section 5, appear to be qualitatively consistent with this mechanism. In the cumulonimbus cloud on 21 November, high ice particle concentrations (>300 per litre) consisting mostly of columnar crystals were observed between -3 and $-8\,^{\circ}$C and some graupel was present. In the 'chimney-type' cloud on 3 May 1988 only relatively modest ice particle concentrations (<10 per litre) were observed and millimetre-sized graupel was not present. Both clouds had a temperature at the top of $-12\,^{\circ}$C, and the droplet spectra in the riming–splintering temperature zone were nearly the same in the two clouds ($>25\,\text{cm}^{-3}$ of droplets $>23\,\mu$m diameter). However, closer scrutiny of the observations reveals problems in quantitatively explaining the high ice particle concentrations observed on 21 November in terms of the riming–splintering process (e.g. Mossop 1985c). In polar maritime cumuliform clouds this mechanism will produce about a factor of ten increase in ice particle concentrations every 10 minutes (Mossop 1985b). By contrast, in this paper we have documented that in similar clouds the concentrations of ice particles increase by factors of 100–1000 in less than 10 minutes.

We can use the results from the laboratory experiments of ice-splinter production during riming to estimate the concentrations of ice particles that should have formed owing to the fall of millimetre-sized graupel through the riming–splintering zone of the small cumulonimbus cloud on 21 November. The laboratory experiments have yielded three rates for splinter production. The rates that have been given for $-5\,^{\circ}$C are: (i) one ice splinter for every 200 drops $>23\,\mu$m diameter that rimed (Mossop 1976), (ii) 75 splinters per mg of rime due to the simultaneous accretion of $>23\,\mu$m and $\leq 13\,\mu$m diameter droplets (Mossop 1978, 1985b, 1985c), and (iii) those derived from the nomogram provided by Mossop (1978) concerning the number of accreted droplets $\leq 13\,\mu$m and $>23\,\mu$m diameter (extrapolated to the $10\,\text{cm}^{-3}$ concentrations of small droplets in the maritime clouds we studied on 21 November).

We have assumed that the collection efficiency for droplets $>23\,\mu$m diameter by a 1.25 mm graupel particle falling at $1.5\,\text{m s}^{-1}$ is 0.5 (after Mossop 1976), and the collection efficiency for the $<13\,\mu$m diameter droplets is 0.2 (Pruppacher and Klett 1980). Graupel ≥ 1 mm in diameter was present in an average concentration of 0.16 per litre over contiguous regions up to 500 m wide just upwind from and adjacent to the region where high concentrations of small ice particles were detected on 21 November. The highest concentrations of millimetre-sized graupel recorded on a single PMS 2-D precipitation probe strip in this region was 0.83 per litre. This strip of images was accumulated in 0.1 second, or over a path length of only ~9 m. The mean diameter of graupel ≥ 1 mm in diameter falling within the riming-splintering zone was 1.25 mm, which falls at $1.5\,\text{m s}^{-1}$ (Locatelli and Hobbs 1974). Only 5 of the 56 graupel particles ≥ 1 mm diameter imaged by the PMS 2-D precipitation probe in this 500 m wide zone were larger than 2 mm in diameter. The concentrations of droplets with diameters $>23\,\mu$m and ≤ 13 mm diameter used in the calculations were the averages of droplets of this size measured with the PMS FSSP probe during two penetrations of the high liquid water content region of this cloud within the riming–splintering zone; these averages were 50 and $10\,\text{cm}^{-3}$, respectively.

Mossop (1978) observed in laboratory experiments that 75 splinters were produced per mg of rime at −5 °C for a maritime-type droplet spectrum, a spectrum nearly identical to that in the maritime clouds we studied. We use 50 splinters per mg of rime to take into account the sharp drop in splinter production outside of the −4 to −6 °C temperature regions, and because the small cumulonimbus cloud that we observed had fewer (about half as many) droplets ≤13 μm diameter in the riming–splintering zone than did Mossop's laboratory cloud. We assume that the ice splinters produced in the riming–splintering zone were dispersed into the adjacent volume of cloud downwind, where the highest concentrations of small ice particles were observed. From our aircraft measurements, this cloud volume was estimated to be at least 2 km downwind by 1 km in the crosswind direction by 0.9 km deep (covering the temperature range from −10 to −3 °C).

Using the facts and assumptions listed above, the concentrations of ice particles produced at 600 s in the downwind cloud volume by the three rates of splinter production from the laboratory experiments listed previously are 5.7, 1.3 and 0.3 per litre, respectively. (The time period of 600 s was chosen since over 90% of the single ice crystals measured in the downwind cloud volume had maximum dimensions between 100 and 600 μm, which, based on the diffusional growth rates of needles, sheaths and hollow columns, shows that they had formed in the previous 2–9 minutes.) The average concentration of ice particles in the downwind (nearly glaciated) volume was 124 per litre (which does not include particles <100 μm in maximum dimension). Thus, ice particle concentrations produced by the riming–splintering mechanisms are calculated to be about two orders of magnitude less than the concentrations of ice particles that developed in this cloud in less than 10 minutes.

Since graupel shafts can be localized in filaments from a few to tens of metres wide (HR), it could be argued that we never penetrated the regions where graupel was present in the highest concentrations. However, if we increase the concentration of graupel in the calculations until the measured concentration of ice particles (124 per litre) is produced, we obtain a required concentration of millimetre-sized graupel of 11 per litre over a path length of 500 m. We have never observed millimetre-sized graupel with such a high concentration in maritime clouds, not even in one PMS 2-D precipitation-probe strip, let alone over a path of several hundred metres. Hence, it appears difficult to explain the high concentrations of small ice particles that we measured in the maritime cumulonimbus cloud that we sampled on 21 November 1988 in terms of the riming–splintering process as it is formulated at present (e.g. Mossop 1985c). However, these calculations are highly sensitive to the number of rimed particles required to produce an ice splinter, now believed to be between 200–250. Our calculations suggest that this discrepancy could be eliminated if the rate were 20–25 particles for one splinter.

There is further evidence that casts doubt on riming–splintering as the primary process responsible for the high ice particle concentrations that we have measured. We have routinely observed high ice particle concentrations (10^2 to 10^3 above those expected from the ice nucleus concentrations) near the tops of clouds where the temperatures are between −10 and −18 °C. If riming–splintering were the responsible process, columnar crystals would have had to be transported to cloud top from the −3 to −8 °C region below, as well as filling the riming–splintering zone itself with crystals. However, the crystal types observed in the tops of these clouds were generally not columnar, instead they were usually crystal habits compatible with having formed and grown *in situ* (viz. hexagonal plates, stellars and dendrites).

If riming–splintering were the dominant ice-forming process in these clouds, one would expect the −3 to −8 °C region to be glaciated and cloud tops between −10 to −18 °C to contain somewhat lower concentrations of columnar crystals together with a

small number of plates and stellars (e.g. Koenig 1977). Except for one instance (5 July 1988), when high concentrations of columnar crystals were carried upward in unusually vigorous maritime convection (Hobbs and Rango 1990), we have not encountered this type of ice crystal distribution.

It should also be noted that in our previous studies of stratiform clouds (nimbostratus, stratocumulus, and altocumulus), ice enhancement was observed but these clouds did not contain graupel, and often the liquid water cloud from which the ice crystals formed was outside of the temperature bounds for the riming–splintering process (HR).

Finally, on various occasions we have sampled continental clouds that exhibited ice enhancement but did not have the requisite concentrations of $>23\,\mu$m diameter droplets in the riming–splintering zone, although $>23\,\mu$m diameter droplets were present above this zone near the cloud top.

While the arguments presented above indicate that the riming–splintering process (as formulated at present) is not a major contributor to the rapidly formed high concentrations of ice particles measured in the upper regions of the small polar maritime cumuliform clouds that we studied, we do not question that, under appropriate conditions, this process may contribute importantly to ice particle concentrations in other regions of the clouds.

(*b*) *Contact nucleation*

Hobbs and Rangno (1985) postulated that contact nucleation (Rau 1950), associated with the flux of aerosol particles driven to the surface of evaporating drops by thermophoretic forces (e.g. Slinn and Hales 1971; Young 1974a; Cooper 1974), might be responsible for the high concentrations of ice particles observed near the tops of aging cumuliform clouds. The flux of aerosol particles to the drops might also be enhanced by electrostatic forces in the following way. The initially high liquid water contents (1 to $2\,g\,m^{-3}$) near cloud tops will tend to reduce the electrical conductivity of the cloudy air (e.g. Pruppacher 1973) and allow the build-up of electrostatic charge on the drops. This in turn could increase (by about an order of magnitude) the collection efficiencies of cloud and precipitation-sized drops for aerosol particles with diameters between 0.02 and $4\,\mu$m (Pruppacher and Klett 1980).

In this paper, and in HR, we have reported that the first ice particles that appear near cloud top are frozen drizzle-sized drops in concentrations of a few per litre over distances of several hundred metres to a kilometre and in concentrations of tens per litre in localized filaments tens of metres wide. Since contact nucleation is particularly effective for drops of this size at temperatures $\geq -10\,°C$ (e.g., Blanchard 1957; Gokhale and Goold 1968; Gokhale and Lewinter 1971; Gokhale and Spengler 1972; Pitter and Pruppacher 1973), this mechanism could be responsible for the frozen drops. Some support for this contention has been put forth recently by Rosinski *et al.* (1987) and Krauss *et al.* (1987). However, it seems less likely that contact nucleation plays a direct role in the second stage of ice production, which is characterized by the sudden appearance of large numbers of small, pristine, vapour-grown ice crystals.

(*c*) *Time-delayed ice nucleation*

Since ice nuclei may be activated stochastically, it has been suggested that ice nucleus measurements may underestimate the activity of ice nuclei in clouds where much longer times are available for nucleation than are generally used in measuring ice nuclei (e.g. Vonnegut 1987). However, our observations indicate that time-delayed nucleation is not an important effect beyond a few minutes. Rather, it appears that once suitable conditions exist in a cloud, ice particles appear in high concentrations almost spontaneously, and

thereafter the concentrations do not increase significantly. Also, as we have reported previously (HR), long-lived, quasi-stationary stratiform clouds, such as fair-weather stratus clouds with tops between −10 and −19 °C and with narrow droplet spectra, do not exhibit ice particle concentrations significantly different from measured ice nucleus concentrations.

We note with interest the reports of Vali (1971) and Vali and Stansbury (1966) concerning the freezing of drizzle drops composed of rain water at temperatures ≥ -10 °C and under conditions of steady cooling. The results of these experiments are relevant to the freezing of drizzle drops in cloud tops that rise or hold their altitude, also to the precipitation form called 'sleet'.[3] Sleet forms when the depth of the layer below the freezing point is $\gtrsim 1$ km. This means that the freezing of these drizzle drops requires about 5–10 minutes, or roughly the same time that the drizzle drops in polar maritime cumuliform clouds are below −5 °C before they freeze and the first stage of ice formation begins.

(*d*) *Nucleation at high supersaturations with respect to water*

Supersaturations in clouds are not measured. Instead, it is generally assumed, on the basis of droplet growth by condensation in simple cloud models, that the supersaturations do not exceed about 1% with respect to liquid water (e.g. Mason 1971). Consequently, in measuring ice nucleating activity, atmospheric aerosols are generally exposed only to water saturation. Indeed, in most experimental arrangements, it is difficult to produce supersaturations significantly in excess of water saturation. Therefore, when it is stated that ice particle concentrations in a cloud are significantly in excess of ice nucleus measurements, the latter refer to measurements made close to water saturation, which are represented, on average, by Eq. (1).

There is mounting evidence that the activity of ice nuclei increases markedly as the humidity rises above water saturation (e.g., Gagin 1972; Rosinski *et al.* 1975; Schaller and Fukuta 1979; Tomlinson 1980; Hussain and Saunders 1984; DeMott and Grant 1984; Gagin and Nozyce 1984; Al-Naimi and Saunders 1985; Khorguani 1985; Blumenstein *et al.* 1987). For example, both Tomlinson and Hussain and Saunders found that the concentrations of ice nuclei increased by about an order of magnitude as the supersaturation with respect to water was increased from 5 to 10%.

There are several ways in which relatively high supersaturations with respect to water may be produced in natural clouds. Supersaturations with respect to water might reach as high as 15–25% at about −20 °C within the vicinity of a freezing drop (Dye and Hobbs 1968; Nix and Fukuta 1974). Similarly, during the growth of graupel, the freezing of rimed droplets may produce supersaturations with respect to water up to ~8% at −10 °C and even greater supersaturations at lower temperatures (Fukuta and Lee 1986). However, since the high supersaturations produced in this manner will affect only very small volumes of air, it is unlikely that they are responsible for the observed high ice particle concentrations.

Numerical modelling studies of clouds have suggested that pockets of high supersaturations may exist in cumuliform clouds (e.g. Clark 1973; Young 1974b; Grabowski 1989). Of particular interest are the numerical modelling results of Young (1974b) and Ochs (1978). This model, which included the growth of drops by condensation and collision–coalescence, predicted the usual small rise in water supersaturation just above cloud base, but, in addition, there was a much larger peak in supersaturation higher up in the cloud. The second peak was associated with the initiation of the collision–

[3] 'Sleet' is used here in the American sense to indicate rain that freezes while falling through a layer of air near the ground with temperatures between about −3 to −10 °C.

coalescence process. As a few drops grew large enough to collect smaller droplets efficiently, the total concentrations of droplets fell abruptly. This reduced the total surface area of the droplets on to which water vapour could condense. Consequently, the supersaturation in the rising parcel of air rose sharply, and, according to Young's calculations for a maritime cloud droplet spectrum, the supersaturation with respect to water reached values up to ~15%. Combining this result with the previously mentioned dependence of ice nucleus activity on supersaturation, we see that in localized regions of a maritime cloud where drops are growing rapidly by collisions, ice particles might be nucleated in far higher concentrations than those that would be nucleated at water supersaturation.

As shown schematically in Fig. 14, the scenario just outlined is consistent with several of our findings for small, polar maritime cumuliform clouds including:

(i) The spontaneous appearance of small vapour-grown ice crystals in high concentrations with habits appropriate to the ambient temperature.
(ii) The appearance of crystals in localized pockets or strands.
(iii) The good correlation between high ice particle concentrations and the breadth of the cloud droplet size distribution (as measured by the threshold diameter, D_T) from which the ice forms. In this connection, we note that Huffman (1973) found in the laboratory experiments that the concentration of ice nuclei (N) is given by:

$$N = cS^{\alpha} \tag{3}$$

where, c and α are constants and S the supersaturation over ice; α ranged from 3 (in rural air) to 8 (in urban air). If S were proportional to D_T, then Eq. (2) would follow from Eq. (3), and the exponent in Eq. (2) might be somewhere between 3 and 8 (compared to our derived value of 4.5).
(iv) The highest concentrations of ice particles (>900 per litre) observed in the present field studies occurred on 5 July 1988 (Hobbs and Rangno 1990). These high concentrations were observed just below a slowly ascending cloud top in a line of clouds that produced an extensive radar echo (prior to the onset of the ice phase and below the region where the ice formed so prolifically) because of the collision–coalescence growth of rain.
(v) The absence of a prolific ice-forming stage in narrow, 'chimney-type' clouds. (Rapid entrainment of dry air into these narrow clouds, while aiding the freezing of drizzle drops, may inhibit the development of high supersaturations.)

Hence, ice nucleation in the presence of supersaturations significantly in excess of water saturation offers a potentially attractive explanation for the sudden formation of high ice particle concentrations that characterize the second ice-forming stage in maritime cumuliform clouds. To test this theory, more information is required on the dependence of ice nucleation on supersaturation (extending up to water supersaturations of the order of 10%), and more sophisticated numerical model calculations should be carried out to investigate further the peak supersaturations that might be achieved in localized regions (~10 m) in clouds.

7. Concluding remarks

This study, together with that reported by HR and Hobbs and Rangno (1990), provides a fairly comprehensive description of the development of ice particles in small

maritime, cumuliform clouds. These studies have revealed a two-stage ice-forming process. In the first stage, a portion (~10–50%) of the drizzle-sized drops freeze near cloud top. This leads to ice particle concentrations of a few per litre. The second ice-forming stage, which appears mainly in the middle and upper regions of clouds with $D \gtrsim 3$ km, is characterized by the extremely fast and prolific production of vapour-grown ice crystals in a large volume. This produces ice crystals in concentrations of tens to hundreds per litre (>100 per litre in the case described in this paper) in about 10 minutes. Thereafter, the ice particle concentrations (and liquid water) decline as the crystals grow by vapour deposition, aggregate and fall out.

The rapid formation of the vapour-grown crystals occurs almost simultaneously with the appearance of the frozen, drizzle-sized drops. In fact, the growth of drops by coalescence apppears to drive the second prodigious ice-forming stage. The rate at which the second stage of ice formation proceeds does not appear to be explicable in terms of the riming–splintering hypothesis as it is formulated at present.

While processes for the formation of the high ice particle concentrations are still speculative, we have suggested that contact nucleation of drizzle-sized drops might be responsible for the first stage of ice development, and that localized pockets of high supersaturation with respect to water could cause the activation of relatively high concentrations of ice nuclei that produce the second ice-forming stage. The pockets of high supersaturations in clouds might be produced during the growth of drops by collisions.

Some additional support for the role of high supersaturations in the production of high ice particle concentrations is provided by the similarity between the rapid production of small vapour-grown ice crystals in high concentrations in maritime cumuliform clouds and the ice crystals that are produced artificially by dry-ice seeding and by the passage of an aircraft through supercooled clouds (Rangno and Hobbs 1983, 1984). In the case of dry-ice seeding, the rapid decrease in temperature produced by the dry ice produces high supersaturations. In the case of aircraft flying in clouds, the expansion of air in the vicinity of propellers and by air flowing over the wings also produces sharp cooling and increases in supersaturation; the supersaturation of the air is enhanced also by water vapour in the engine exhausts. It seems probable, therefore, that in all three cases high supersaturation is the cause of rapid formation of ice crystals in high concentrations.

Acknowledgements

We thank our pilots and members of our flight crew for helping to collect the data. Thanks are also due to B. Baker for encouraging us to look more carefully at 'chimney-type' clouds, to Dr M. Baker for useful discussions, and to Dr J. Rosinski for analysing the millipore filters. This research was sponsored by a grant from the National Science Foundation.

This paper is dedicated to Dr Stanley C. Mossop (1922-1987), who did so much to focus attention on the problem of ice in clouds.

References

Al-Naimi, R. and Saunders, C. P. R. 1985 Measurements of natural deposition and condensation-freezing ice nuclei with a continuous flow chamber. *Atmos. Environ.*, **19**, 1871–1882

Blanchard, D. C. 1957 The supercooling, freezing and melting of giant water drops at terminal velocity in air. Pp. 233–247 *in Artificial Simulation of Rain*. Ed. H. Weickmann. Pergamon Press, New York

Blumenstein, R., Rauber, R. M., Grant, L. O. and Finnegan, W. G. 1987 Application of ice nucleation kinetics in orographic clouds. *J. Clim. Appl. Meteorol.*, **26,** 1363–1376

Braham, R. R., Jr. 1964 What is the role of ice in summer rain showers? *J. Atmos. Sci.*, **21,** 640–645

Clark, T. L. 1973 Numerical modeling of the dynamics and microphysics of warm cumulus convection. *J. Atmos. Sci.*, **30,** 857–873

Clayden, A. W. 1905 *Cloud Studies*, Pp. 110–111. William Clowes and Sons, Ltd., London

Coons, R. D. and Gunn, R. 1951 Relation of artificial cloud-modification to the production of precipitation. Pp. 235–241 in *Compendium of Meteorology*. American Meteorological Society, Boston

Cooper, W. A. 1974 A possible mechanism for contact nucleation. *J. Atmos. Sci.*, **31,** 1832–1837

DeMott, P. J. and Grant, L. O. 1984 Development of ice crystal concentrations in stably stratified orographic cloud systems. Pp. 191–194 in Preprint Vol., *Ninth Int. Conf. Cloud Phys.* Tallin, Estonia, Acad. Sci. USSR

Dye, J. E. and Hobbs, P. V. 1968 The influence of environmental parameters on the freezing and fragmentation of suspended water drops. *J. Atmos. Sci.*, **25,** 82–96

Fletcher, N. H. 1962 *The Physics of Rainclouds*, Pp. 241–242. Cambridge University Press

Fukuta, N. and Lee, H. J. 1986 A numerical study of the supersaturation field around growing graupel. *J. Atmos. Sci.*, **43,** 1833–1843

Gagin, A. 1972 The effect of supersaturation on ice crystal production by natural aerosols. *J. Rech. Atmos.*, **6,** 175–185

Gagin, A. and Nozyce, H. 1984 The nucleation of ice crystals during the freezing of large supercooled drops. *J. Rech. Atmos.*, **18,** 119–129

Gokhale, N. R. and Goold, J. Jr. 1968 Droplet freezing by surface nucleation. *J. Appl. Meteorol.*, **7,** 870–874

Gokhale, N. R. and Lewinter, O. 1971 Microcinematographic studies of contact nucleation. *J. Appl. Meteorol.*, **10,** 469–473

Gokhale, N. R. and Spengler, J. D. 1972 Freezing of freely suspended, supercooled drops by contact nucleation. *J. Appl. Meteorol.*, **11,** 157–160

Goldsmith, P, Gloster, J. and Hume, C. 1976 The ice phase in clouds. Pp. 163–167 in Preprint Vol., *Int. Conf. Cloud Phys.* Boulder, Colorado

Grabowski, W. W. 1989 Numerical experiments on the dynamics of the cloud-environment interface: small cumulus in a shear-free environment. *J. Atmos. Sci.*, **46,** 3513–3544

Hallett, J. and Mossop, S. C. 1974 Production of secondary ice particles during the riming process. *Nature*, **249,** 26–28

Hallett, J., Sax, R. I., Lamb, D. L. and Ramachandra Murty, A. S. 1978 Aircraft measurements of ice in Florida cumuli. *Q. J. R. Meteorol. Soc.*, **104,** 631–651

Heymsfield, A. J. and Hjelmfelt, M. R. 1984 Processes of hydrometeor development in Oklahoma convective clouds. *J. Atmos. Sci.*, **41,** 2811–2835

Hobbs, P. V. 1969 Ice multiplication in clouds. *J. Atmos. Sci.*, **26,** 315–318

1974 High concentrations of ice particles in a layer cloud. *Nature*, **251,** 694–696

Hobbs, P. V. and Atkinson, D. A. 1976 The concentrations of ice particles in orographic clouds and cyclonic storms over the Cascade mountains. *J. Atmos. Sci.*, **33,** 1362–1374

Hobbs, P. V. and Farber, R. 1972 Fragmentation of ice particles in clouds. *J. Rech. Atmos.*, **6,** 245–258

Hobbs, P. V. and Rangno, A. L. 1985 Ice particle concentrations in clouds. *J. Atmos. Sci.*, **42,** 2523–2549

1987 Reply to comments on "Ice particle concentrations in clouds". *J. Atmos. Sci.*, **44,** 911–915

1990 Rapid development of high ice particle concentrations in small polar maritime cumuliform clouds. *J. Atmos. Sci.*, **47** 2710–2722

Hobbs, P. V., Funk, N. T., Weiss, R. W., Sr., Locatelli, J. D. and Biswas, K. R.	1985	Evaluation of a 35 GHz radar for cloud physics research. *J. Atmos. Ocean Tech.*, **2**, 35–48
Huffman, P. J.	1973	Supersaturation spectra of AgI and natural ice nuclei. *J. Appl. Meteorol.*, **12**, 1080–1082
Hussain, K. and Saunders, C. P. R.	1984	Ice nucleus measurement with a continuous flow chamber. *Q. J. R. Meteorol. Soc.*, **110**, 75–84
Khorguani, V. G.	1985	Ice forming behaviour of atmospheric aerosols. Pp. 114–121 in *J. Hydrol. Meteorol.*, Acad. Sci. USSR
Knollenberg, J. A.	1981	Techniques for probing cloud microstructure. Pp. 15–91 in *Clouds, their Formation, Optical Properties and Effects*. Eds. P. V. Hobbs and A. Deepak. Academic Press
Koenig, L. R.	1963	The glaciating behavior of small cumulonimbus clouds. *J. Atmos. Sci.*, **20**, 29–47
	1977	The rime-splintering hypothesis of cumulus examined using a field-of-flow cloud model. *Q. J. R. Meteorol. Soc.*, **103**, 585–606
Kraus, T. W., Bruintjes, R. T., Verlinde, J. and Kahn, A.	1987	Microphysical and radar observations of seeded and nonseeded continental cumulus clouds. *J. Clim. Appl. Meteorol.*, **26**, 585–606
Locatelli, J. D. and Hobbs, P. V.	1974	Fall speeds and masses of solid precipitation particles. *J. Geophys. Res.*, **79**, 2185–2197
Locatelli, J. D., Hobbs, P. V. and Biswas, K. R.	1983	Precipitation from stratocumulus clouds affected by fallstreaks and artificial seeding. *J. Clim. Appl. Meteorol.*, **22**, 1393–1403
Magono, C. and Lee, C. W.	1966	Meteorological classification of natural snow crystals. *J. Fac. Sci., Hokaido University, Japan, Ser. VII*, **2**, 321–335
Mason, B. J.	1971	*The Physics of Clouds*, pp. 128–136. Oxford University Press, London
Mossop, S. C.	1976	The production of secondary ice particles during the growth of graupel by riming. *Q. J. R. Meteorol. Soc.*, **102**, 45–57
	1978	The influence of the drop size distribution on the production of secondary ice particles during graupel growth. *Q. J. R. Meteorol. Soc.*, **104**, 323–330
	1985a	Ice particle concentrations in clouds. *Bull. Am. Meteorol. Soc.*, **66**, 264–273
	1985b	The microphysical properties of supercooled cumulus clouds in which an ice particle multiplication process operated. *Q. J. R. Meteorol. Soc.*, **111**, 183–198
	1985c	Secondary ice particle production during riming growth: the effect of drop size distribution and rimer velocity. *Q. J. R. Meteorol. Soc.*, **111**, 1113–1124
Mossop, S. C. and Hallett, J.	1974	Ice crystal concentrations in cumulus clouds: influence of the droplet spectrum. *Science*, **186**, 632–634
Mossop, S. C., Ruskin, R. E. and Heffernan, K. J.	1968	Glaciation of a cumulus at approximately −4 °C. *J. Atmos. Sci.*, **25**, 889–899
Mossop, S. C., Ono, A. and Wirhart, E. R.	1970	Ice particles in maritime clouds near Tasmania. *Q. J. R. Meteorol. Soc.*, **96**, 487–508
Mossop, S. C., Cottis, R. E. and Bartlett, B. M.	1972	Ice crystal concentrations in cumulus and stratocumulus clouds. *Q. J. R. Meteorol. Soc.*, **98**, 105–123
Nix, N. and Fukuta, N.	1974	Non-steady-state kinetics of droplet growth in cloud physics. *J. Atmos. Sci.*, **31**, 1334–1434
Ochs, H. T.	1978	Moment conserving techniques for warm cloud microphysical computations. *J. Atmos. Sci.*, **35**, 1959–1973
Pitter, R. L. and Pruppacher, H. R.	1973	A wind tunnel investigation of freezing of small water drops falling at terminal velocity in air. *Q. J. R. Meteorol. Soc.*, **99**, 540–550
Pruppacher, H. R.	1973	Electrofreezing of supercooled water. *Pure Appl. Geophys.*, **104**, 623–634
Pruppacher, H. R. and Klett, J. D.	1980	*Microphysics of Clouds and Precipitation*, D. Reidel Pub. Co., Holland
Rangno, A. L. and Hobbs, P. V.	1983	The production of ice particles by aircraft. *J. Clim. Appl. Meteorol.*, **22**, 214–232
	1984	Further evidence for the production of ice particles by aircraft. *J. Clim. Appl. Meteorol.*, **23**, 985–987

Rau, W.	1950	Über die Wirkungsweise der Gerfrierkerne im unterkuhlen Wasser. *Zeit. Naturforsch.*, **5a,** 667–675
Rosinski, J. and Morgan, G. M.	1988	Ice-forming nuclei in Transvaal, Republic of South Africa. *J. Aerosol. Sci.*, **19,** 531–538
Rosinski, J., Nagamoto, C. T. and Kerrigan, T. C.	1975	Heterogeneous nucleation of water and ice in the transient supersaturation field surrounding a freezing drop. *J. Rech. Atmos.*, **9,** 107–117
Rosinski, J., Haagenson, P. L., Nagamoto, C. T. and Parungo, F.	1987	Nature of ice-forming nuclei in marine air masses. *J. Aerosol. Sci.*, **18,** 291–309
Schaller, R. C. and Fukuta, N.	1979	Ice nucleation by aerosol particles: experimental studies using a wedge-shaped ice thermal difusion chamber. *J. Atmos. Sci.*, **36,** 1788–1802
Slinn, W. G. and Hales, J. M.	1971	A re-evaluation of the role of thermophoresis as a mechanism of in- and below-cloud scavenging. *J. Atmos. Sci.*, **28,** 1465–1471
Tomlinson, E. M.	1980	'A new horizontal gradient, continuous flow, ice thermal diffusion chamber and detailed observation of condensation-freezing and deposition nucleation.' Ph.D. Dissertation, Department of Meteorology, University of Utah
Turner, F. M., Radke, L. F. and Hobbs, P. V.	1976	Optical techniques for counting ice particles in mixed-phase clouds. *Atmos. Tech.*, **8,** 25–31
Vali, G.	1971	Quantitative evaluation of experimental results on the heterogeneous freezing nucleation of supercooled liquids. *J. Atmos. Sci.*, **28,** 402–409
Vali, G. and Stansbury, E.J.	1966	Time-dependent characteristics of the heterogeneous nucleation of ice. *Can. J. Phys.*, **44,** 477–502
Vonnegut, B.	1987	Importance of including time in the specification of ice nucleus concentrations. *J. Clim. Appl. Meteorol.*, **26,** 322
Young, K. C.	1974a	The role of contact nucleation in ice phase initiation in clouds. *J. Atmos. Sci.*, **31,** 768–776
	1974b	The evolution of the drop spectra through condensation, coalescence, and breakup. Pp. 95–98 in *Am. Meteorol. Soc. Conf. Cloud Phys.*, Tucson, Arizona